

**This manuscript is a EarthArXiv preprint** and has been submitted and revised for publication in **Tectonics** and has not yet been formally accepted for publication. Subsequent versions of this manuscript may, thus, have slightly different content. When formally accepted, the final version of this manuscript will be available via the 'Peer-reviewed Publication DOI' link on the right-hand side of this webpage. Please feel free to contact anyof the authors; we warmly welcome feedback.

# **The Merluza Graben: how a failed spreading centre influenced margin structure, and salt deposition and tectonics in the Santos Basin, Brazil**

\*Leonardo M. Pichel<sup>1</sup>; Christopher A-L Jackson<sup>1</sup>; Frank Peel<sup>2</sup>; Oriol Ferrer<sup>3</sup>

*1. Basins Research Group (BRG), Department of Earth Science and Engineering, Imperial College London, London, SW7 2BP, UK*

*2. The University of Texas at Austin, Bureau of Economic Geology, Jackson School of Geosciences, Austin, TX, USA*

*3. Department de Geodinàmica i Geofísica, Facultat de Geologia, Universitat de Barcelona, C/Martí i Franquès s/n, 08028 Barcelona, Spain*

## Abstract

The relative timing between crustal extension and salt deposition can vary spatially along passive margin salt basins as continents unzip, or as the locus of extension shifts towards the embryonic ocean spreading centre. Determining the relative timing of salt deposition, rifting, and seafloor spreading is often problematic due to the diachronous nature of rifting, the ability of salt to fill pre-existing topography, and the subsequent flow and deformation of that salt. We here use 2D PSDM seismic data and structural restorations to investigate the Merluza Graben, a large rift-related depocentre located in the southern, most proximal part of the Santos Basin, Brazil along-strike of a failed spreading centre, the Abimael Ridge. The graben is defined by up to 3.5 km of base-salt relief along its basinward-bounding fault and internal base-salt horsts that are up to 1 km high. This compartmentalises deformation, producing intra-graben extensional and contraction salt structures, ramp-syncline basins, and expulsion rollovers, resulting in a remarkably different salt-tectonic structural style to that seen in the adjacent areas. We also conduct structural restorations to analyse the spatial and temporal evolution of salt-tectonic structural styles and the relationship this has to potential prolonged crustal extension in the Merluza Graben. This approach further constrains local variations in the relative timing of rifting and salt deposition, and the impact this has on salt tectonics along the margin. The results of our study can be applied to better understand the tectono-stratigraphic development of other salt-bearing rifted margins.

## 1. Introduction

Passive margin salt basins commonly form at the transition from the late syn-rift to early post-rift stages (Jackson and Vendeville, 1994; Warren 2016; Rowan 2014; Jackson and Hudec, 2017). Examples include South Atlantic basins such as those offshore Brazil (Mohriak et al., 1995; Davison et al., 2012; Garcia et al., 2012; Jackson et al., 2015b; Pichel et al., 2018, 2019c), West Africa (Marton et al. 2000; Hudec and Jackson, 2004; Peel 2014), NW Africa (Davison 2005; Tari and Jabbour, 2013; Pichel et al., 2019a), Nova Scotia and Newfoundland (Adam and Krezsek, 2012; Deptuck and Kendell, 2017), the Gulf of Mexico (Peel et al., 1995; Rowan et al., 2004; Hudec et al., 2013; Hudec et al., 2019) and the Red Sea (Rowan 2014). In many of these basins, the timing of salt deposition varies laterally from syn- rift (i.e., during the bulk of crustal extension) to post-rift (i.e., after the bulk of crustal extension ceased); this diachroneity can occur as the timing of rifting and break-up varies along-strike as continents “unzip” (cf. Northern and Southern Red Sea, Augustin et al., 2014; Rowan 2014), or as the locus of rift-related extension shifts basinward towards the embryonic spreading centre. In the latter, case, salt deposited in proximal areas after crustal faulting had ceased would be called “post-rift”, whereas age-equivalent salt deposited in more distal areas during ongoing crustal faulting and extension would be defined as syn-rift (e.g., the South and Central Atlantic salt basins; Rowan, 2014; 2020; Tari et al., 2017).

Because of the diachroneity in tectonics and deposition, it can be difficult to determine the relative timing of salt deposition, rift-related fault activity, and seafloor spreading (Hudec et al., 2013; Pindell and Kennan, 2007; Rowan 2014; 2020; Marton et al., 2000; Karner and Gambôa, 2007; Mohriak et al., 2008; Davison et al., 2012; Quirk et



al., 2013; Norton et al., 2016; Curry et al., 2018) (cf. Peron-Pindivic and Manatschal, 2009; Huismans and Beaumont, 2011; 2014). Another challenge relates to the fact that salt thickness variations may arise due to passive infilling of relief inherited from the pre-salt (pre-depositional) rift phase or formed during (syn-depositional) and/or after salt deposition (post-depositional) (Davison et al., 2012; Lewis et al., 2013; Pichel et al. 2018). Passive margin salt basins also undergo gravity-driven deformation (Rowan, 2014; Peel; 2014; Jackson and Hudec, 2017), which further masks their original distribution and thickness and, consequently, the timing of salt deposition relative to thick-skinned extension. Where the base-salt relief is significant, post-rift salt deformation is also influenced by inherited rift topography (Ferrer et al., 2014; Dooley et al., 2016; 2018; Dooley and Hudec, 2016; Roma et al., 2018; Pichel et al., 2018; 2019b-c, Evans and Jackson, 2020). This typically produces multiphase salt deformation characterized by coeval zones of contraction and extension (Dooley et al., 2016; 2018; Pichel et al., 2019b-c), as well as sigmoidal, asymmetric minibasins formed by salt-detached overburden translation above base-salt ramps (i.e., ramp-syncline basins, Jackson and Hudec, 2005; Pichel et al., 2018).

The salt-influenced Santos Basin, offshore SE Brazil captures much of the tectonic and depositional complexity described above. It is the largest (c.  $3.5 \times 10^5$  km<sup>2</sup>) and widest (>520 km) salt basin in the Atlantic Ocean (Fig. 1a-b) (Lentini et al., 2010; Davison et al., 2012; Kumar et al., 2013). It is nearly twice the width of the largest salt basin offshore Africa, the Kwanza Basin, Angola (c. 300 km; Lentini et al., 2010; Kukla et al 2018) and it is noticeable that its conjugate, the Namibe/Benguela basins contain little to no salt (cf. Blaich et al., 2011; Moulin et al., 2012; Heine et al., 2013, Kukla et al., 2018). The Santos Basin contains a thick (average depositional thickness of c. 2.5 km) Aptian salt layer deposited above prominent and complex base-salt relief (Fig. 1b)

(Garcia et al., 2012; Davison et al., 2012; Rodriguez et al., 2019; Pichel et al., 2018, 2020b). This relief is primarily associated with the hydrocarbon-rich Tupi and Sugar Loaf Highs in the São Paulo Plateau, its deep marginal basin, and the proximal Merluza Graben (Garcia et al., 2012; Davison et al., 2012; Gomes et al., 2009; Pichel et al., 2018; 2019b). The basin is also affected by a complex rift and break-up history, with the development of a failed seafloor spreading centre, the Abimael Ridge, in its southern portion as rifting shifted abruptly basinward towards Africa (Fig. 2-3) (cf. Blaich et al., 2011; Scotchmann et al., 2006; 2010; Mohriak et al., 2010; Heine et al., 2013; Kukla et al., 2018).

For these reasons, the Santos Basin is the one of the most complex salt basins in the South Atlantic, with many as-yet unresolved controversies. Some of these debates revolve around the regional kinematics and dynamics (e.g., the Albian Gap; Mohriak et al., 1995; Quirk et al., 2012; Jackson et al., 2015a,b; Pichel et al., 2019c; Pichel and Jackson 2020b), and the syn- vs. post-salt nature of salt-related deformation (Davison et al., 2012; Fiduk and Rowan, 2012, Quirk et al., 2012; Jackson et al., 2015b). Other controversies relate to the water depth of during salt deposition, and the variable timing of crustal deformation and seafloor spreading relative to salt deposition and subsequent flow (Karner and Gambôa, 2007; Mohriak et al., 2008; Davison et al., 2012; Rodriguez et al., 2019; Kukla et al., 2018). Previous studies have not explicitly addressed the impact of the failed seafloor spreading centre on salt deposition and subsequent deformation. We thus expand on these works to investigate the largest rift-related depocentre in the Santos Basin, the Merluza Graben.

The Merluza Graben is located at the northward continuation of the failed seafloor spreading centre, the Abimael Ridge (Figs. 2-3), in the southern, proximal part of the

basin, within the salt-tectonic domain dominated by gravity-driven extension (Davison et al., 2012; Quirk et al., 2012; Pichel and Jackson, 2020b) (Fig. 1b). The Merluza Graben is not itself defined as a failed spreading centre, but simply as a rift-related depocenter located ahead of and that laterally passes into one; given their close spatial relationship, we argue below that the structure and evolution of the Merluza Graben is genetically related to processes that formed the Abimael Ridge further south. Up to 3.5 km of structural relief is present in association with the Merluza Graben at the base-salt due to the presence of graben-bounding normal faults. Some authors suggest that this relief is largely the product of post-salt (i.e., post-Aptian) normal fault displacement (Scotchman et al., 2010) whereas others argue that it is simply a consequence of inherited topography from the pre-salt (i.e., Barremian-Aptian) rifting (Garcia et al., 2012; Lebit et al., 2019). Irrespective of the timing of deformation, the Merluza Graben is also geometrically distinct from other salt-related structural provinces in the basin. It has a significantly greater base-salt relief defined by very large displacement (>2 km) normal faults as opposed to the minor (~ 0.5 km) relief observed on the São Paulo Plateau and other parts of the basin. In comparison with other areas of the Santos Basin, the Merluza Graben has been relatively understudied (cf. Mohriak et al. 2010; Garcia et al 2012; Rowan et al., 2019; Magee et al., 2020). However, it represents an important setting in which to understand salt tectonics along large rift-related structures as well as the interplay between diachronous rifting, and salt deposition and deformation along rifted passive margins.

To understand the 3D geometry and kinematics of the Merluza Graben, and its influence on salt deposition and deformation, we combine interpretations of closely-spaced, (8 x 4 km), 2D post stack depth-migrated (PSDM) seismic reflection profiles with balanced structural restorations. We aim to answer the following questions: 1)

what is the relative timing of rifting, and salt deposition and deformation in and around the Merluza Graben? 2) how did the growth of large extensional structure impact regional salt tectonics along a rifted margin? and 3) how can our revised model for the syn- to post-rift tectono-stratigraphic evolution of the Merluza Graben help us better understand the geological evolution of the Santos Basin and its conjugate? These questions are not only applicable to the Santos Basin, but also to other rifted margins salt basins worldwide.

## **1. Geological Setting**

The Santos Basin is bound by the Cabo Frio Arch to the northeast and by the Florianopolis Platform to the southwest (Mohriak et al., 1995; Garcia et al., 2012). The basin formed in response to Early Cretaceous rifting which eventually led to the opening of the South Atlantic (e.g., Meisling et al., 2001; Modica and Brush, 2004; Karner and Gambôa, 2007; Mohriak et al., 2008). Rifting was characterized by ESE-SE extension and development of NNE-NE-oriented grabens and half-grabens filled by syn-rift Barremian, fluvial-lacustrine deposits. Syn-rift deposits are overlain by an early-to-middle Aptian, carbonate-dominated sag sequence (Meisling et al., 2001; Davison et al., 2012).

Rifting and breakup were complex, with apparently several aborted attempts during the early Aptian to extend seafloor spreading northwards of the Pelotas Basin and Florianopolis Fracture Zone (FFZ) from an area of oceanic crust (Meisling et al. 2001; Gomes et al. 2009; Scotchman et al., 2006; 2010) (Figs. 2-3). According to plate reconstructions (Fig. 2a), seafloor spreading had already initiated to the north (Espírito Santo and Campos basins) and south (Pelotas Basin) of the Santos Basin (and Merluza Graben) during the early to mid-Aptian, i.e., before the onset of salt

deposition (cf., Scotchmann et al., 2008; 2010; Moulin et al., 2012; Heine et al., 2013). By the late Aptian-Albian boundary, at the end of salt deposition in the Santos Basin, only the Santos-Namibe/Benguela segments had not yet broken up. During the early Albian, the Basins were then completely broken apart with the abandonment of the southern spreading centre coming from the Pelotas Basin and shift of spreading eastward towards Africa (Fig. 2b). This complex rift propagation resulted in various syn- to post-rift intrusive and volcanic features in the southwestern Santos Basin, in the Abimael Ridge (Mohriak et al., 2008; 2010), and further northwards around the Merluza Graben (Magee et al., 2020). It also produced a 2-4 km thick syn-rift and the hydrocarbon-rich, pre-salt sag succession above stretched continental crust on the São Paulo Plateau to the east (Gomes et al., 2009; Scotchman et al., 2006; 2010).

The Merluza Graben, the area focus of this study, is the northward continuation of a linear negative gravity anomaly in the southwestern and most proximal portion of the Santos Basin, the Abimael Ridge (Fig. 3a). According to the 3D gravity-inversion and subsidence analysis of Scotchman et al. (2006; 2010), this anomaly corresponds to a “tongue” of thin (c. 5 km, fig. 3b), oceanic crust transitioning northwards into an extremely thinned, highly-stretched and weakened continental to transitional crust underneath the Merluza Graben. The Merluza Graben is thus interpreted to have formed due to extensional stresses transmitted from the attempted northward propagation of the failed spreading centre (Mohriak et al., 2010).

Regional fault activity decreased during Aptian times in most of the basin and by the Late-Aptian, a c. 2.5 km thick (on average) salt succession was deposited (Davison et al., 2012; Garcia et al., 2012; Pichel and Jackson, 2020b). Due to the asymmetric nature of continental break-up caused by a late Aptian shift in the locus of rifting

towards Africa (cf. Meisling et al., 2001; Scotchman et al., 2010), no salt was deposited in the conjugate margin (i.e., the Namibe-Benguela Basin; Lentini et al., 2010; Kukla et al., 2018). In the Santos Basin, salt deposition was controlled by relief inherited from the preceding rift event, resulting in marked spatial variations in original salt thickness (Davison et al., 2012; Garcia et al., 2012; Rodriguez et al. 2019). In pre-salt lows such as the Merluza Graben and the deep marginal trough, salt was potentially up to 3.5 km thick (Fig. 1b) (Garcia et al., 2012; Lebit et al., 2019). Conversely, on pre-salt highs such as the Outer High in the São Paulo Plateau (Fig. 1b), salt was only c. 1.5-2.5 km thick (Garcia et al., 2012; Davison et al., 2012; Rodriguez et al., 2019).

During the early Albian, continental break-up and the emplacement of oceanic crust resulted in thermally induced, post-rift subsidence, a rise in eustatic sea-level, and the establishment of fully marine conditions in the Santos Basin (Quirk et al., 2012). This promoted widespread deposition of a carbonate-dominated succession (Fig. 1b) (Modica & Brush, 2004). During the late Albian, the basin tilted south-eastward, inducing gravity gliding of the salt and its overburden. Salt-related deformation produced numerous thin-skinned, predominantly basinward-dipping, salt-detached normal faults that dismembered the Albian carbonate platform into rafts in the updip extensional domain (zone of extension, Fig. 1) (Demercian et al., 1993; Cobbold et al., 1995; Guerra and Underhill, 2012; Quirk et al., 2012). Post-Albian sedimentation was characterized by margin-scale clastic progradation, with sediments derived from the uplifting Serra do Mar mountain range (Fig. 1a) (Modica & Brush, 2004). Most late Albian faults in the updip extension domain became inactive by the end of Albian and deformation migrated downdip into the Albian Gap, a large counter-regional (i.e., basinward-dipping) rollover (Jackson et al., 2015a, Pichel and Jackson, 2020), and further eastwards onto the São Paulo Plateau (Fig. 1) (Quirk et al., 2012) (Pichel et

al., 2019c). Post-Albian salt tectonics was characterized by basinward salt expulsion from the Albian Gap, local salt welding (Davison et al., 2012; Jackson et al., 2014; 2015a), and up to c. 30 km of overburden translation and related salt inflation further downdip on the São Paulo Plateau (Pichel et al., 2018).

Salt tectonics was influenced by the base-salt relief and salt thickness variations associated with the inherited rift topography (Garcia et al., 2012; Pichel et al. 2018, 2019b-c). This was especially important in the intermediate translational domain on the São Paulo Plateau, above the Outer High, with the development of ramp-syncline basins and broadly coeval contraction, extension, and passive diapirism (Pichel et al., 2018; 2019c). Due to the complex rifting and break-up history of the Santos Basin, the base-salt relief is also significant in other areas such as its deep salt basin (cf. Davison et al. 2012), and the proximal Merluza Graben and Albian Gap (cf. Pichel and Jackson, 2020). Salt flow partition and structural variability within the basin may thus be regionally even more complex than previously described.

### **3. Dataset and Methods**

#### **3.1. Seismic Data and Interpretation**

We use an extensive (c. 76,000 km<sup>2</sup> areal coverage), zero-phased processed, Kirchhoff pre-stack depth-migrated (PSDM) 2D seismic dataset covering nearly the entire length of the Santos Basin and the Albian Gap (Fig. 1a and c). The 2D survey comprises NW- and NE-trending profiles that are oriented sub-parallel to the dip- and strike-direction, respectively, of the basin and the central and northern parts of the Merluza Graben (Figs. 1c). The seismic dataset has a relatively dense line spacing (c. 4 km and 8 km between dip- and strike-orientated profiles, respectively), giving it a

quasi-3D character at the regional scale. Seismic profiles have a total record length of 16 km and we display images following the Society of Economic Geologists (American SEG) normal polarity convention, whereby a downward increase in acoustic impedance is represented by a positive reflection event (white on greyscale seismic sections) and a decrease in acoustic impedance by a negative event (black on greyscale seismic section) (Brown, 2011). Given the location of the Merluza Graben in the southern portion of the basin, we focus our analysis on the southernmost half of the survey (Fig. 1c).

We mapped base- and top-salt (red) based on their distinct seismic expression and overburden geometries (pink polygon in Figs. 6-11). As we did not have direct access to borehole data, mapping of key post-salt horizons was based on their tectono-stratigraphic significance (i.e., erosional unconformities) and their distinct growth strata geometries (i.e., onlaps and downlaps). Approximate age-calibration of our seismic-stratigraphic analysis was provided by comparing our seismic profiles to recently published, borehole-constrained, seismic profiles in Garcia et al. (2012), Guerra and Underhill (2012), Quirk et al. (2012), Hadler-Jacobsen et al. (2014), and Jackson et al. (2015a). We mapped the Top Albian unconformity (blue), a seismic reflection defining the top of the post-salt sequence deposited during the first stages of salt movement (dark blue horizon in Figs. 6-11). This unconformity outlines the geometry and extent of the Albian Gap, which partially overlaps with the Merluza Graben in the south (Figs. 4 and 6). We also mapped a Paleogene unconformity (yellow horizon in Figs. 6-11) that marks the end of bulk salt deformation across most of the basin (cf. Garcia et al., 2012; Guerra and Underhill, 2012; Jackson et al., 2015b). Five key Upper Cretaceous-Paleocene horizons in and around the Merluza Graben were also mapped to constrain its structural style, and pre- and post-salt kinematics.



### 3.2. Restorations

To restore geometries imaged on seismic reflection profiles we combine decompaction and unfolding by simple vertical shear and move-on-fault algorithms, following established restoration workflows for salt-related deformation (cf. Rowan and Ratliff 2012). We restore two of the most representative and best-oriented profiles (i.e., parallel to both the rift- and salt-related tectonic transport direction) imaging the Merluza Graben. Post-salt horizons are unfolded to a gently-dipping, clinoform-like seabed geometry, characteristic of the prograding clastic slopes identified in this part of the basin (cf. Modica and Brush, 2004; Hadler-Jacobsen et al. 2010). This workflow thus incorporates more realistic geometries than previous studies by reconstructing the paleo-seabed through time using the present seabed as a template, and local erosional unconformities and toplaps as additional constraints (cf. Garcia et al., 2012; Pichel and Jackson, 2020b).

We also incorporate flexural isostatic compensation during each step of decompaction of the stratigraphic succession. This allows us to quantify and remove the effects of differential loading and basin subsidence, and to provide more accurate estimates of the base-salt geometry, associated salt thickness, and post-salt deformation through time (Pichel and Jackson 2020b). The decompaction is performed using the Sclater and Christie (1980) function and assumes a carbonate (Albian) and siliciclastic (post-Albian) overburden, in agreement with data presented from elsewhere in the basin (Guerra and Underhill, 2012; Hadler-Jacobsen et al., 2010). For the flexural isostasy we use a crustal density of  $2.78 \text{ g/cm}^3$  and lithospheric elastic thickness ( $T_e$ ) of 5 km. We also test  $T_e$  values of 1.5, 10 and 15 km but choose  $T_e = 5 \text{ km}$  as we and others (Scotchman et al., 2006; 2010; Davison et al., 2012) argue this is a more valid

approximation for highly-stretched continental crust; the same value has been applied by other studies focused on the geodynamic evolution of the Santos Basin (Garcia et al., 2012; Rodriguez et al., 2019).

## **4. Results**

### **4.1. Basement Structure**

The Merluza Graben is c. 160 km long in our study-area but it extends c. 50 km further south (Figs. 1 and 3). It trends NNE in the south and NE for c. 40 km in the north. It has an average width of 15-20 km, reaching up to 45 km at its central-north portion (Fig. 4 and 5). The structure has been previously described simply as a “graben”, based primarily on the interpretation of one or two seismic profiles (Mohriak et al. 2010; Garcia et al., 2012), but in reality, it is a much more complex. Its proximal flank has an average relief of c. 0.5 km associated with basinward-dipping (i.e., SE-dipping) normal faults. Its distal flank has an average relief of c. 1 km (Figs. 6 and 9-10), but which reaches up to c. 3.5 km at its central-north portion due to the presence of a large, landward-dipping (i.e., NW-dipping) normal fault system (herein named the Merluza Fault) (Figs. 7 and 8). These faults strike N-NE, with individual segments being c. 20-30 km long and seemingly separated by relay ramps (Figs. 4a and 5). For these reasons, the Merluza Graben has a variable and complex cross-sectional geometry, i.e., it is a relatively symmetric graben in its north and south portions (Figs. 6 and 11), becoming more asymmetric and with significantly greater (>2 km) base-salt relief where it is widest near its centre (Figs. 7-10). Where the Merluza Fault has >3 km of throw, the Merluza Graben has a classical half-graben geometry in which the base-salt within and updip of the graben represent a single, large (c. 40-50 km wide), basinward-dipping hangingwall slope (Figs. 7 and 8).

The Merluza Graben contains numerous secondary faults (Figs. 4a and 5a). These faults have a dominant NE-SW strike and landward dip in the northern sector but are more variable in the central and southern sectors, with NE- and NW-trending sets defining numerous intra-basin horsts (Figs. 4a and 5a). At both its proximal and distal margins, small (c. 2-4 km wide and 4-18 km long) horsts also occur (Fig 5a). Overall, the amount and size of faults offsetting the base-salt decreases northward and eastward within and away from the Merluza Graben (Fig. 4). It is also important to note that the base-salt dips regionally basinward in the southern part of the Santos Basin where the Merluza Graben is present (i.e., both within and updip of the Merluza Graben, and downdip in the adjacent Albian Gap (Figs. 1b and 4; see also Figs. 7-9). This is in stark contrast with the central and north portions of the Santos Basin, where the proximal base-salt dips regionally landward within and around the Albian Gap (cf. Davison et al., 2012; Pichel and Jackson, 2020b).

## **4.2. Salt and supra-salt styles**

### **4.2.1. Updip of the Merluza Graben**

Updip from the Merluza Graben, near the proximal edge of the Santos Basin, numerous salt rollers (R, Figs. 6, 7 and 9) occur in an area of thin (c. 300 m) to nearly-welded (<50 m) salt, the base of which dips basinward. These rollers are defined predominantly by basinward-dipping listric normal faults and landward-dipping rollovers (Figs. 6-9 and 11), although a few are bound by landward-dipping normal faults (Fig. 7). Based on the age of their hangingwall growth strata, the rollers formed immediately after salt deposition, during early Albian times, and were active until the earliest Late Cretaceous (LC1) (Figs. 6, 7, 9 and 10).

These rollers transition basinward into landward-thickening sigmoidal strata of Albian-LC1 age that are not directly in contact with any salt rollers and/or related salt-detached normal faults, i.e., they occur above a broadly flat, undeformed top-salt (Figs. 6, 9 and 10). These packages of strata are c. 4-8 km wide, 8-15 km long, and overlie, a basinward-dipping base-salt ramp (Figs. 12a-b and 13a-b). They can be gently folded and they are truncated at their tops at their downdip ends by prominent erosional unconformities (yellow arrows, Figs. 6-11). In places, these strata are tilted ( $>30^\circ$ ) basinward as indicated by their top unconformities being steeper than their internal strata (yellow arrows, figs. 7 and 8). These characteristics indicate that these growth strata are formed by c. 4-8 km of translation above basinward-dipping base-salt ramps and are, thus, defined as ramp-syncline basins (RSBs; cf. Jackson and Hudec, 2005; Pichel et al., 2018).

#### **4.2.2. Merluza Graben**

At the updip, NW edge of the Merluza Graben, deformation is characterized by contractional structures and development of Albian-LC1 salt anticlines (Figs. 6 and 9), which transition along-strike into 4-6 km tall, considerably younger (LC4-Paleogene) squeezed diapirs (Figs. 7 and 13a-b). In places, however, especially in the south where the base-salt is more variable in terms of relief, the updip edge of the Merluza Graben is characterized by a LC1-4 basinward-thickening extensional rollover associated with a landward-dipping normal fault (Figs. 10 and 13b). Its underlying Albian strata are, however, upturned and thinned against the salt (Fig. 10), suggesting that the structure originated in response to early (i.e., Albian) contraction and salt inflation as seen elsewhere in the study-area.

Within the Merluza Graben itself, early deformation (Albian-LC1) varies more significantly along-strike than elsewhere. In the northern part, early deformation in updip areas is characterized by horizontal translation and the development of RSBs (Figs. 6-8), whereas contraction and the formation of salt anticlines typifies downdip areas (Figs. 6-7). Some of these early anticlines and inflated salt bodies evolved into large, >8.5 km tall salt stocks during the latest Cretaceous-Paleogene (Fig. 8), probably by a combination of active and passive diapirism (see section 4.3).

During the latter part of the Late Cretaceous (LC2-LC5), deformation was characterized by the development of large, >15 km long, and up to 3.5 km thick, basinward-thickening rollovers (Figs. 6-8, 12c-d and 13c). These can vary from being dominantly extensional when they occur in direct contact with the Merluza Fault (Fig. 7), or dominantly driven by expulsion where they display a more sigmoidal shape and are in direct contact with diapirs (Fig. 8). They can also have a more hybrid character, being variably influenced by both processes through time (Fig. 6), as seen further downdip in the Albian Gap (cf. Pichel and Jackson 2020b). Where the Merluza Fault base-salt relief is small (<1 km), mid-Late Cretaceous (LC2-5) deformation was dominated by basinward salt expulsion beyond the Merluza Graben (Figs. 6 and 10). Where the base-salt relief was greater (>1 km), LC2-3 strata were largely confined within the Merluza Graben (Figs. 8, 9 and 11), suggesting that basinward salt expulsion and consequent salt inflation and diapirism was spatially restricted to within the depocentre.

In the Merluza Graben's southern portion, deformation is more complex than in the north, with a greater number of diapirs and/or salt rollers (Figs. 9-11). Where rollers occur within the graben, they are commonly bound by 1-4 km tall, landward-dipping

listric faults that formed during the latest Cretaceous (LC 2-5) to Paleogene (Fig. 10). These rollers are not capped or flanked by Albian-to-LC1 strata, suggesting that during this time the area was occupied by salt in the form of a large diapir that likely represented the southern continuation of the structure originally defining the Albian Gap (cf. Mohriak et al., 1995; Jackson et al., 2015; Pichel and Jackson, 2020b). At its southernmost portion, where the Merluza Graben has a more variable pre-salt relief, the area is characterized by numerous 4-5 km tall diapirs and equally thick minibasins (Fig. 11). They present classic halokinetic sequences (i.e., near-diapir upturn and thinning strata, cf. Giles and Rowan, 2012; Pichel and Jackson, 2020a) indicating that they formed primarily by passive diapirism. As seen by their relatively thick (0.6-1 km) roofs uplifted above a regional datum, these diapirs have also been influenced by late, latest Cretaceous-Paleogene shortening.

### **4.3. Restorations**

Two of the most representative and ideally oriented cross-sections (i.e., orthogonal to the main trend of pre-salt and salt structures; Fig. 4) have been restored to constrain the complex and highly variable, salt-related kinematics in the Merluza Graben. These restorations allow us to quantify deformation style (i.e., extension, translation and contraction), how these varied through time and space, and their relationship with the Merluza Graben base-salt relief. Additionally, we use discrepancies in salt area/volume (where they occur, Fig. 14) to understand the ambiguous temporal relationship between salt deposition and rift-related fault activity (cf. Davison et al., 2012; Lewis et al., 2013; Rowan and Jarvie, 2020).

#### **4.3.1. Section A**

The first restored section has the largest base-salt structural relief (c. 3.5 km) on the Merluza Fault (Figs. 8 and 14). For this reason, early (Albian-LC3) salt deformation updip of and within the Merluza Graben is completely decoupled from salt deformation further downdip (Fig. 8), with salt and overburden not translating beyond the Merluza Fault (Fig. 14). We therefore restore deformation only within and above the Merluza Graben, with a pin being located above its basinward edge (Fig. 14a-f). In some of the earlier stages, however, the pin is located further updip due to local variations of salt flow caused by salt depletion beneath thick minibasins and/or expulsion rollovers (Fig. 14g), or by base-salt relief (Fig. 14h-i). We do not restore slip on the Merluza Fault as constraining its timing and kinematics from seismic observations alone is highly problematic (cf. Lewis et al., 2013; Jackson and Hudec, 2017). We, nonetheless, use discrepancies in the restored salt area to analyze if and when the fault was still active after salt deposition (see section 4.3.2).

Our restorations suggest that during the Albian (Fig. 14i), salt rollers and basinward-dipping listric faults accommodated c. 2.5 km of extension updip of the Merluza Graben within the section. These rollers pass downdip into an Albian minibasin where the base-salt is more rugose, and a 2-3 km wide passive diapir further downdip above a small horst defining the updip edge of the Merluza Graben. We interpret this diapir to have formed initially by salt inflation driven by local buttressing of salt flow against the base-salt high. Further downdip, over the Merluza Graben, another Albian minibasin formed as salt and overburden translated downdip over the basinward-dipping hangingwall of the Merluza Fault (Fig. 14i). As shown on seismic data (Fig. 8), these minibasins present a highly asymmetric, landward-thickening growth strata characteristic of RSBs. From the distance of their lowermost onlaps against the top of the basinward-dipping ramp, we estimate that they accommodate 3.5-4 km of

basinward translation. This indicates that the immediately adjacent passive diapir accommodated c. 1 km of cryptic extension (cf. Vendeville and Jackson, 1992; Jackson and Hudec, 2017), widening after an initial phase of inflation (Fig. 14i). Basinward translation of salt and overburden down and onto the hangingwall of the Merluza Fault resulted in localized overburden contraction and additional salt inflation (Fig. 14i). Where salt was buried by Albian sediments, 1-2 km wide salt anticlines formed, whereas further downdip where no Albian was deposited, a large passive diapir developed (Fig. 14i).

Subsequent deformation (LC1-LC2) was accommodated by ongoing salt-detached extension (c. 5.5 km in total) that was primarily accommodated by the most proximal normal fault ( $F_1$ , Fig. 14g-h). It is also likely that this fault accommodated additional 1.5 km of extension updip of the section during deposition of LC3. During LC1,  $F_1$  accommodated c. 3 km of extension. Extension also occurred further downdip in the form of widening of the intermediate passive diapir above the updip edge of the Merluza Graben. As in the previous stage, this cryptic extension is constrained by the fact that we observe a total of 4.5 km of translation downdip within the LC1 RSB strata (Fig. 8). Given this translation would require the same amount of updip extension, we infer c. 2 km of diapir widening in addition to the 3 km of extension accommodated by the normal fault  $F_1$ . Downdip, near the Merluza Fault, deformation was characterized by continuous passive diapirism due to the lack of deposition above the inflated salt. During LC2, extension (c. 2 km) over the  $F_1$  was accommodated by shortening and squeezing of the central diapir as the system became partially pinned due to salt depletion underneath the downdip minibasin (Fig. 14g-h). Translation was halted and the Albian-LC1 RSB switched to a LC2 expulsion rollover with salt being expelled



basinward into the downdip diapir and, as a consequence, the older RSB strata rotated downward (Figs. 8 and 14g).

Minor updip (out-of-section) extension is inferred in the following stage (LC3) by additional shortening/narrowing (c. 1.5 km) of the intermediate diapir (Fig. 14f). However, during LC3, the overall style of deformation changed to being dominated by margin progradation and amplification of the expulsion rollover, with consequent amplification of the downdip passive diapir adjacent to the Merluza Fault. By the end of LC3, the system was pinned and no more extension or translation occurred within the overburden (Fig. 14f). This was caused by salt evacuation from the source-layer, thickening of minibasins as well as sediment progradation and overburden thickening downdip of the Merluza Graben. As a result, the following stages (LC4-7 and Pg) of deformation were characterized by passive diapirism with only minor (c. 1.2 km) contraction and diapir squeezing. This is indicated by the extra section length of overburden strata (Fig. 14a-e) and their significant near-diapir upturn (Fig. 8 and 14). Minor shortening and the predominant vertical growth of diapirs occurred due to the 5-8 km thick overburden deposited in minibasins within and beyond the Merluza Graben (Fig. 8), effectively pinning the system. The two previous diapirs were squeezed; the initially narrower diapir became welded at the end of Cretaceous (LC7-LC8), whereas downdip the wider diapir developed an upward-flaring shape without welding (Fig. 8 and 14).

In summary, the restoration of Section A depicts a total of c. 8 km of extension and c. 8 km of translation during Albian-LC1, constrained by normal fault growth strata and RSBs respectively. This is also kinematically-balanced by downdip contraction against the Merluza Fault, which is mostly cryptic (i.e., accommodated by diapir squeezing

and active rise) due to the lack of overburden deposition. From LC2 onwards the style of deformation changed and becomes more laterally constrained as the salt layer thins and the overburden thickens. This results in limited extension balanced entirely by diapir squeezing updip of the Merluza Graben, and salt expulsion and inflation within the Merluza Graben. The restoration also demonstrates complex, multi-stage deformation in the Meruza Graben, characterized by the temporal reversal of strain patterns typical of areas influenced by significant base-salt relief (cf. Dooley et al., 2018; Pichel et al., 2019b; Erdi and Jackson, 2020). For example, the central diapir, located over the updip edge of the Merluza Graben, likely originated in response to early Albian inflation driven by the buttressing of salt flow against the updip edge of the Merluza Graben, eventually reaching the surface to become a passive diapir. Continuous inflation and thickening allowed local salt flow to accelerate, with the passive diapir widening by c. 3 km by the end of Albian-LC1 (Fig. 14i and h). From LC2 onwards, this diapir narrowed as it became pinned due to depletion of its source-layer, thickening of the downdip overburden and, regionally, by buttressing against the Merluza Fault.

#### **4.3.2. Section B**

Section B is located further north, where the Merluza Fault base-salt relief is modest (c. 0.5 km) and, as a consequence, salt was able to flow downdip beyond the restored section (Figs. 8 and 15). Similar to Section A, the overburden is pinned in different locations through time within (Fig. 15b-c) or at the basinward edge of the Merluza Graben (Fig. 15d-e), due to salt depletion from underneath thick minibasins and expulsion rollovers.

The style of deformation updip of the Merluza Graben is similar to Section A; this is not surprising, given the majority of structures in this section are the laterally equivalent to the larger features seen further south (Figs. 4, 14 and 15). Albian deformation is characterized by c. 4 km of updip extension and c. 7 km translation, the latter represented by the development of a c. 7 km wide RSB (Fig. 15e). The inferred amount of translation is c. 3 km greater than the measured extension likely due to extension occurring updip beyond our study-area (Fig. 15d-f). This updip extension and translation resulted in a c. 2 km wide salt anticline that formed in response to contraction as salt flow was partially buttressed against the horst at the updip edge of the Merluza Graben (cf. Section A; Figs. 14 and 15). Additional contraction and salt inflation occurred further downdip, against and beyond the Merluza Fault.

Nonetheless, Section B differs from Section A because basinward salt flow was only partially buttressed so that salt was able to flow downdip beyond the Merluza Fault (out-of-section) as its base-salt relief was significantly smaller. This explains why both early extension and translation are around twice that observed in Section A (Fig. 14). During LC1, two salt rollers developed updip of the Merluza Graben and accommodated an additional c. 2.5 km of extension. Another RSB formed downdip of the central anticline, indicating that both salt and overburden translated basinward by c. 5 km (Fig. 15d). This suggests that an additional c. 2.5 km of proximal extension occurred further updip, beyond the studied section. The central salt anticline and the downdip passive diapir downdip were amplified due to continuous salt expulsion from underneath the RSB and adjacent minibasins (Fig. 15d). Continuous subsidence and thickening of these minibasins, and the related depletion and near-welding of underlying salt, halted translation and the system became pinned over the proximal edge of the Merluza Graben during the LC3 (Fig. 15c). Updip extension reduced

significantly (to just 0.6 km) during LC3-LC5 and was mostly accommodated further downdip by amplification of the proximal anticline without visible overburden translation (Fig. 15a-c). Downdip, over the Merluza Graben, salt was gradually expelled basinward beyond the Merluza Graben by the development of a hybrid, expulsion-extensional rollover above the early inflated salt/diapir (Fig. 15a-c). This rollover is part of the larger Albian Gap that extends further downdip and north of the Merluza Graben (Pichel and Jackson 2020b).

#### **4.3.3. Discrepancies in salt area**

A notable feature observed in the restorations is the excess of salt by the end of the workflow (i.e., Aptian). In Section B, the restored salt area is c. 130% of its present-day area whereas in Section A this value is significantly greater (c. 180%). Despite the salt area changing through time in 2D restorations as a consequence of salt flowing in/out of the plane of section and/or dissolution (cf. Rowan and Ratliff, 2012), the discrepancy in Section A is too large to be explained purely by these mechanisms. Another constraint that this discrepancy is not driven by out-of-plane salt flow is the observation that in order to maintain margin-scale salt connection between the Merluza Graben and the Deep Salt Basin (white-dashed line in Fig. 16), the Merluza Graben would require an even greater (c. 5 km) depositional salt thickness. This seems unrealistic given the present-day salt thickness (<0.5 km to welded), the dominant extensional structural style, and lack of very large (>5 km) diapirs in and around the Merluza Graben (Figs. 6-11 and 16). This could suggest that the Merluza Graben and its main bounding fault were active or reactivated after salt deposition (i.e., there was never 180% of the present salt in the graben). Although less likely,

other alternatives are also possible, which we outline and consider in the following sections.

## **5. Discussion**

### **5.1. Rifting and Salt Deposition in the Merluza Graben**

We explore three distinct scenarios that could explain the discrepancies in the restored salt area over the Merluza Graben and its bounding faults: a) differential dissolution, b) underfilling of a pre-existing graben and c) post-salt rifting and fault slip.

In the first scenario, salt would have been preferentially dissolved by the end and/or immediately after its deposition (late Aptian-early Albian) (Fig. 17a). Salt dissolution is a common phenomenon in salt basins (cf. Warren 2016; Jackson and Hudec, 2017) and has been documented in the São Paulo Plateau (cf. Rodriguez et al., 2019), located c. 50 km downdip to our study-area (Fig. 16). Dissolution is likely to have occurred in the Merluza Graben too but was probably incapable of removing a significant salt thickness in the short time (c. 0.5-2 Ma) between the end of salt deposition and deposition of the first Albian sediments. Dissolution is also unlikely to have been greater in the graben than on its downdip footwall (Fig. 17a), which is a requirement to explain the discrepancies in salt area without completely removing salt from the footwall where a suite of salt rollers indicate that salt was originally present (Figs. 7-8). Preferential dissolution is thus unlikely and probably unrealistic.

In the second scenario, the Merluza Fault would have acted as a barrier for water influx, which would have resulted in an underfilled Merluza Graben with consequently thinner salt than its adjacent footwall and São Paulo Plateau (Fig.17b). This is also unlikely as flooding and seawater percolation would have come from the southernmost

part of the basin adjacent to the Merluza Graben and partially connected to the oceanic basin already formed further south in the Pelotas Basin (cf. Davison et al., 2012; Scotchman et al., 2010).

Our third, and preferred hypothesis is that the Merluza Fault was active *after* salt deposition, such that the Merluza graben is presently larger, in terms of cross-sectional area, than the salt it presently contains (Fig. 17c). This would explain most if not all of the discrepancy (c. 180%) between the present-day and restored salt area within the Merluza Graben in Section A. In Section B, the significantly smaller discrepancy (c. 30%) could be primarily attributed to salt being expelled from underneath expulsion-extensional rollovers and flowing downdip beyond the Merluza Fault due to its small (c. 0.5 km) structural relief. Where its relief was greater (> 3 km, figs. 7-8), as in Section A (Fig. 14), salt could not flow beyond the Merluza Fault. Post-salt rifting and crustal extension in the Merluza Graben would reconcile important observations from our seismic data and restored sections, such as the thickening of Late Cretaceous strata (LC3 and 4) towards the Merluza Fault (Figs. 7, 8, 14 and 16). We discuss below how base-salt relief and post-salt crustal extension influenced the post-depositional salt tectonics.

Another process that may have enhanced base-salt relief and offset in the Merluza Fault is salt loading (i.e., syn-depositional salt drainage, Davison et al., 2012; Quirk et al., 2012), in which salt flows towards structural lows during its deposition, amplifying the existing base-salt relief. However, we argue that this process alone cannot explain the observed discrepancy between graben and salt area in the Merluza Graben as it would require the graben to be almost entirely filled with salt by the end of its deposition (see Davison et al., 2012, their figure. 11).

## 5.2. The Merluza Graben and Salt Tectonics

Salt deformation within and updip of the Merluza Graben was partially to completely decoupled from the downdip part of the Santos Basin due to the base-salt relief associated with the Merluza Fault (Figs. 6-11 and 13-15). The earliest (Albian-LC2) salt-related deformation was characterized by clear strain partitioning, with updip extension (i.e., salt rollers), intermediate translation (i.e., ramp-syncline basins), and downdip contraction (i.e., salt inflation and folding) or, where no overburden was deposited, passive diapirism (Figs. 13a-b and 14-15). Contractional structures also formed further updip and were occasionally reactivated by extension (i.e., diapir widening) due to salt flux variations over a base-salt horst (cf. Dooley et al., 2018; Pichel et al., 2019b) at the updip edge of the Merluza Graben (Figs. 6-8, 13a-b and 14-15).

Towards the mid-Late Cretaceous (LC3-4), minibasins at the updip margin of the Merluza Graben started to weld due to rapid margin-scale progradation, minibasin thickening, and the consequent depletion (i.e., welding) of the underlying salt. This resulted in salt inflation further downdip, near the Merluza Fault, a reduction to complete cessation of overburden translation (i.e., gliding) further updip and, consequently, less strain partitioning within the Merluza Graben (Figs. 13c and 14-15). By this time, deformation was dominated from basinward salt expulsion from underneath rollovers and minibasins, and downdip inflation and passive diapirism above the Merluza Fault (Figs. 13c and 14-15). Where its related base-salt relief was large (> 2 km), salt inflation and diapirism were focused within the graben and above the Merluza Fault (Figs. 8 and 14). Where its related base-salt relief was smaller, salt was able to flow downdip beyond the graben (Figs. 6 and 15)

The inferred post-salt crustal extension in the Merluza Fault was largely decoupled from post-salt deformation due to the presence of an initially thick salt (c. 2 km, half of its restored thickness, Fig. 14). This extension must have caused continuous subsidence of the base-salt and basinward tilting of the Merluza Fault hangingwall (Fig. 17c), consequently favouring salt evacuation, and basinward gliding and overburden translation (rollers and RSBs in figs. 6-11). This may have also contributed to salt thickening and passive diapirism over a wide (10-15 km) area above the Merluza Fault and subsequent development of large diapirs (Figs. 8, 10-11 and 14). Progressive base-salt subsidence, driven by slip on the Merluza Fault, may have also favoured salt inflation and passive diapirism without significant salt flowing downdip beyond the bounding structure. Increasing relief may have also suppressed the development of allochthonous salt bodies ahead of the advancing expulsion rollover (Fig. 14).

The kinematics and ultimate structural style of the southern part of the Albian Gap (cf. Pichel and Jackson, 2020b) were also influenced by the development of the Merluza Graben (Figs. 4, 6, 10-12 and 16). Where both the Merluza Graben and Albian Gap intersect, the strike of faults, salt rollers, and post-Albian rollover sequences within the Albian Gap follows the same trend of the sub-salt structure (Fig. 4). In addition, some of the larger passive diapirs and/or inflated salt structures formed above the Merluza Fault seem to have also contributed to the initial and final width of the Gap by as much as 10 km (Figs. 7-8 and 11) (Pichel and Jackson 2020b). Post-salt crustal extension must also have contributed c. 5% (2-3 km) of the present-day width (50-60 km) of the Albian Gap where it overlaps the Merluza Graben.

### **5.3. Timing and Causes of Prolonged Rifting**



### 5.3.1. The Merluza Graben

Due to the ability of salt to flow and fill topography without showing significant evidence of extension when lacking overburden (i.e., deformation is cryptic above passive diapirs, cf. Jackson et al., 2015b), constraining the exact timing of post-salt crustal extension is challenging (Lewis et al., 2013). However, based on the fact that earliest Late Cretaceous growth strata are observed (LC1-LC3, Figs. 7, 10 and 16) adjacent to the Merluza Fault, and the observation that these strata are absent or very thin on its footwall, we infer that the Merluza Fault was active until at least this time. It is also likely that rifting was continuous and, thus, the Merluza Fault and other secondary faults within the Merluza Graben were active during and immediately after salt deposition (i.e., Aptian-Albian). This extension was nonetheless cryptic and mostly accommodated by salt thickening and passive diapirism above the Merluza Fault, as shown by salt and supra-salt geometries in our restorations (Figs. 14-15). We thus infer that thick-skinned extension occurred from the early Aptian (prior to salt deposition) until the early Late Cretaceous (approximately Cenomanian-Turonian), and that it was primarily accommodated by slip on the Merluza Fault.

What could have caused prolonged rifting in the Merluza Graben whereas basinward, less than 40 km away and over >100 km wide area (i.e., the São Paulo Plateau), most faults were inactive and are not associated with substantial (0-0.5 km) base-salt relief (Fig. 16)? We propose that rifting continued locally as a result of reactivation of the aborted spreading centre during and soon after oceanic spreading shifted basinward onto another spreading centre coming from the north (i.e., Campos-Kwanza, Fig. 18). As the Merluza Graben sits at the northern termination of the failed spreading centre and is characterized by highly-stretched and weakened crust (cf. Scotchman et al.,

2010), it was consequently more prone to failure and reactivation than the adjacent structural domains.

### **5.3.2. Rifting and Salt Deposition – A regional evolutionary model**

We also suggest that the São Paulo Plateau and its underlying Outer High originated due to distributed rifting between the two laterally overlapping rift propagators during Barremian-early Aptian times (Figs. 2 and 18a). Subsequently, as the propagators continued to advance, they began to develop a physical connection (the incipient FFZ) so that rifting in the SPP ceased or was drastically reduced (Fig. 18b). The area remained relatively shallower than the adjacent domains of focused rifting locally favouring deposition of the highly-prolific shallow-water carbonates of the pre-salt sequence (cf. Gomes et al., 2009). Whereas the São Paulo Plateau remains largely unfaulted during (late Aptian) and after salt deposition (early Albian) (Fig. 18b), the landward and basinward domains (Merluza Graben and Distal Salt Basin, respectively, Fig. 18) continued to be affected by rifting. This implies that salt deposition was at least partially syn-rift in these domains (Fig. 18b), an assumption supported by their significantly more rugose and faulted base-salt (Fig. 16), which likely resulted in an overall greater depositional salt thickness and mobility. In the hangingwalls of the thick-skinned, rift-related faults (i.e., Merluza Fault), where salt must have been initially >1 km thick, thick-skinned extension was cryptic and mostly accommodated by salt thickening and passive diapirism (Figs. 14-15).

Eventually, the southern spreading centre was abandoned and oceanic spreading fully established basinward of the São Paulo Plateau and Deep Salt Basin with the Florianopolis transform fault connecting the southern and the northern active spreading segments (Fig. 18c). Extensional and strike-slip stresses associated with

this rift jump were not sufficient to affect the relatively thicker and stronger continental crust in the São Paulo Plateau, which remain unfaulted. In the Merluza Graben, due to its highly-stretched and weakened crust, early post-salt rifting continued as extensional stress were transmitted from the newly-formed spreading centre east of the São Paulo Plateau (Fig. 18c).

Our kinematic model works independently of using an unzipping scenario with only one northward-propagating, southern rift propagator (cf. Kukla et al., 2018) or with two (i.e., southern and northern) propagators (cf. Scotchmann et al.; 2010; Moulin et al., 2012; Heine et al., 2013), as long as there is an abrupt shift in spreading towards Africa by the end of salt deposition (Figs. 2 and 18). However, we adopt the two-propagator scenario as it fits recent tight-fit plate reconstructions (Moulin et al., 2012; Heine et al., 2013) and it explains the following geological observations: i) the development of earlier rift basins to the north of Santos (Reconcavo-Tucano-Jatoba, cf., Heine et al., 2013, RTJ in fig. 2); ii) Cenomanian-Turonian breaching of the Walvis-Rio Grande Ridge (Scotchmann et al., 2008); iii) biostratigraphic evidence for marine influence in pre-break up (i.e., Aptian) faunas in West Africa (cf. Blauch et al., 2011; Rowan 2018), and iv) the presence of thicker salt in the Santos Basin compared to elsewhere in the South Atlantic suggesting that the margin was the last to breakup. Moreover, an abrupt shift of seafloor spreading from the south of the Santos Basin towards Africa is geodynamically more easily explained if rifting had already initiated in the north.

#### **5.4 Implications**

This evolutionary model explains the greater dimension and concave geometry of the Santos Basin relative to other South Atlantic salt basins (Campos and Espirito-Santo,

Brazil and Kwanza and Benguela Basin, West Africa). This was caused by pre-salt distributed rifting between the two partially overlapping and interfering spreading centres (i.e., SPP, Fig. 18a) and, ultimately by a shift in the locus of rifting (cf. Mohriak et al., 2008; Scotchman et al., 2010) from the southern spreading centre onto the northern one (Fig. 18b). Our model also helps to reconcile why the conjugate margin (i.e., the Namibe Basin) is salt-poor (Fig. 18c) (cf. Lentini et al., 2010; Kukla et al., 2018); i.e., most of the original salt basin remained attached to the Brazilian margin after the rift jump (Fig. 18c).

Our integrated approach and evolutionary model allowed also an improved understanding of the relationship between diachronous and highly complex rifting and break-up with salt deposition and tectonics along the entire Santos margin. This approach can be applied to other basins to better constrain regional to local variations of sub-salt fault activity relative to salt deposition and tectonics, commonly a challenging task in present-day passive margins such as the Gulf of Mexico, the South Atlantic, Nova Scotia, NW Africa as well as the North Sea, Barents Sea and the Red Sea. In addition, this approach can be used to understand and restore depositional salt thicknesses and sub-salt fault activity in fossil hyperextended margins that are now inverted as part of orogens such as in the Alps, Pyrenees (cf. Roca et al., 2011; Decarlis et al., 2014, Benoit et al., 2020; Burrell and Teixell, 2020; Célini et al., 2020; Ford and Vergés 2020). Moreover, constraining the regional context and variability of salt deposition and sub-salt fault activity can afford an improved understanding of the pre- and post-salt structural framework as well as of the distribution of pre-salt reservoirs and source-rocks. More specifically, our analysis suggests that the relatively thicker syn-rift and sag sequences in the São Paulo Plateau is likely a

consequence of protracted and distributed extension between two overlapping rift propagators.

## **6. Conclusions**

The Merluza Graben acted as a major control on pre-, syn- and post-salt deformation in the Santos Basin due to its location, geometry, size, timing of activity and associated base-salt relief. The style of salt tectonics in the area is markedly different than adjacent structural domains such as the Albian Gap and São Paulo Plateau. This is a consequence of its greater depositional salt thickness and complex base-salt relief as well as its continued, post-salt extension. In the areas of greater base-salt relief on its basinward bounding fault (Merluza Fault) the Merluza Graben behave as a nearly-completely independent salt basin with updip extensional, translational and contractional domains of gravity-driven deformation. This was also the case for the earliest (Albian-LC2) deformation where the Merluza Fault relief was less than 1 km, but, eventually, margin progradation was able to expel salt from the Merluza Graben onto the adjacent Albian Gap and São Paulo Plateau, connecting it with these structural domains. Base-salt relief in the Merluza Graben resulted in contractional structures located within the Santos Basin regional extensional domain. Some of these contractional structures occurred over its updip edge defined by a horst or structural high and were later reactivated by extension. Others formed due to salt inflation and contraction by buttressing against the Merluza Fault and resulted in large squeezed diapirs, some of which the largest in the entire basin.

We combine our kinematic analysis with restorations to show that discrepancies in restored salt thicknesses across rift structures can be used to constrain the relative timing of sub-salt, crustal extensional with salt deposition and, ultimately its impact on

salt tectonics. Prolonged crustal extension occurred locally in the Merluza Graben because it represents the northern continuation of an aborted rift propagator and spreading centre characterized by highly attenuated and, thus, weaker crust that was affected by extensional stresses transmitted from the newly-formed spreading centre further basinward. This extension was largely decoupled from post-salt deformation due to the initially, c. 2 km thick salt but favoured basinward salt evacuation and gliding towards the Merluza Fault due to continuous base-salt subsidence and basinward tilting of its hangingwall.

### **Acknowledgments**

First, we thank TGS and WesternGeco as well as individuals in these companies, in particular Fernando Alvarez, K. Sanchez and E. Vargas, for granting permission to use their *proprietary 2D seismic data*. We also thank Schlumberger for academic licenses of Petrel and Petex for Move. We are also very grateful for the useful discussions with and Eduard Roca-Abella; Ritske Huisman, Rob Gawthorpe, Thomas Theunissen; Gillian Apps, Oliver Duffy. We also thank Christian Heine for providing the plate reconstructions used in figure 2.

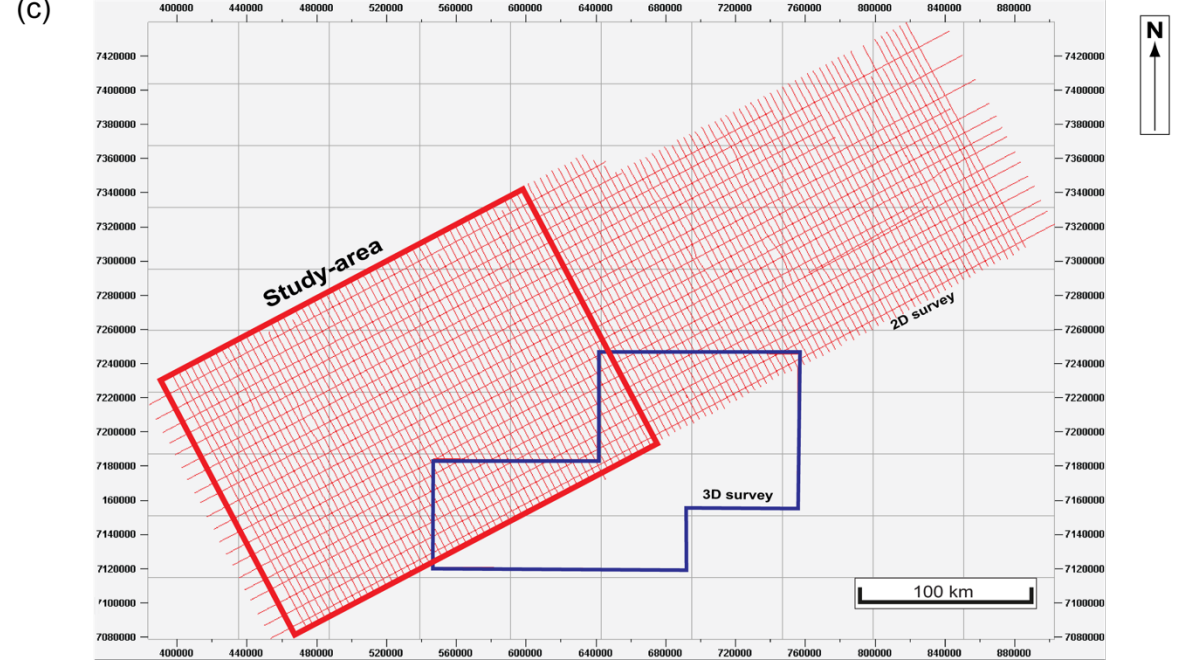
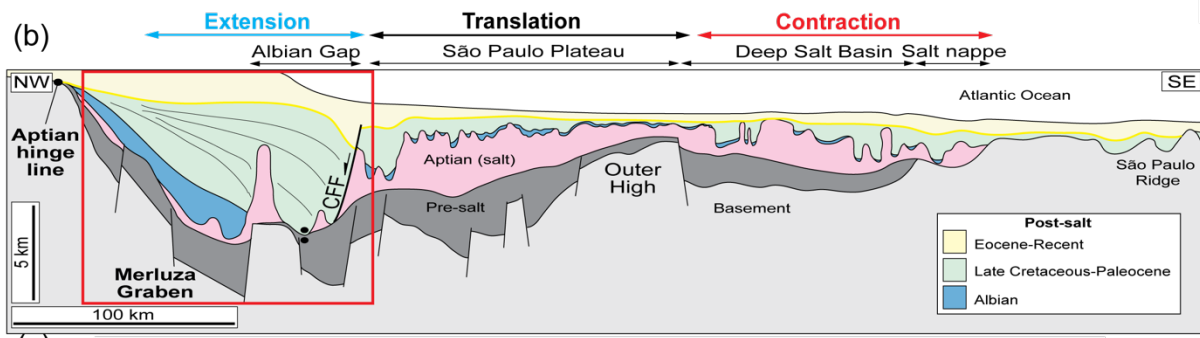
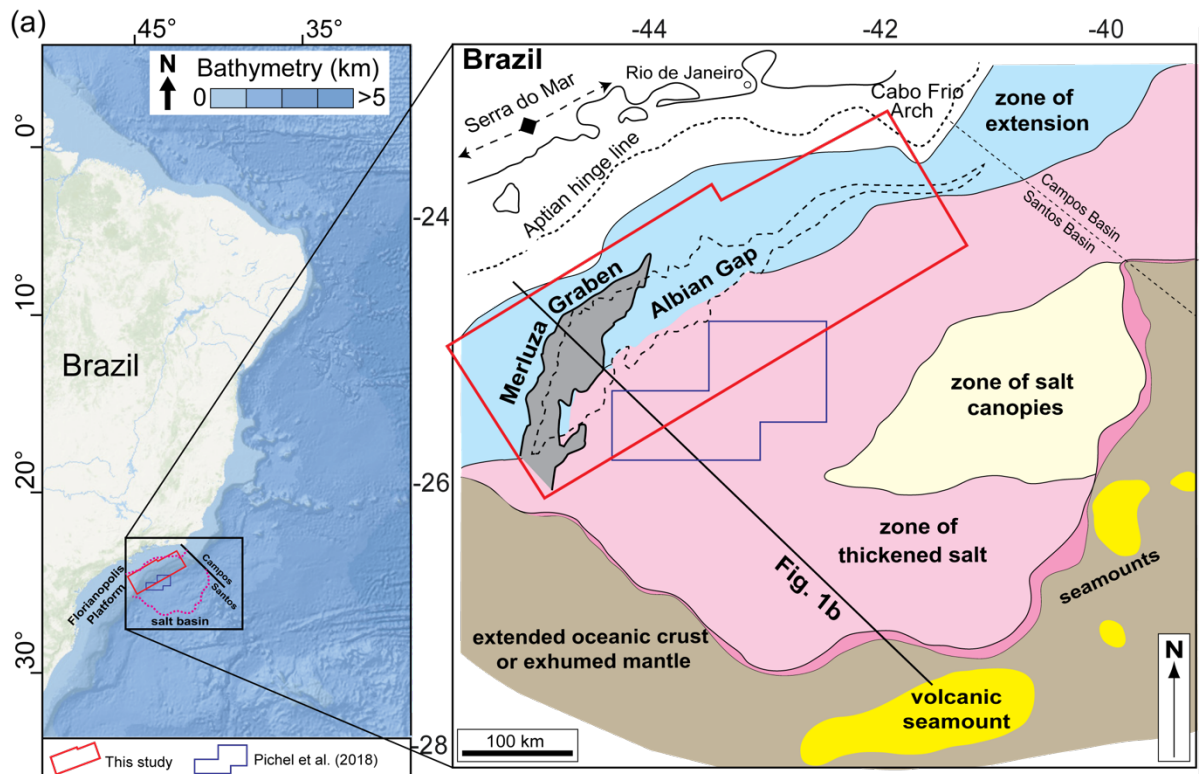


Figure 1: (a) Bathymetry and structural maps showing the regional salt-related structural domains offshore SE Brazil including the Merluza Graben (focus of this study), the Albian Gap and the datasets utilized (adapted from Davison et al., 2012; Pichel and Jackson 2020b). (b) Regional geoseismic cross-section showing the main regional salt-related structural domains offshore the Santos Basin and our study-area in a red polygon (adapted from Jackson et al. 2015b). CFF refers to the Cabo Frio Fault bounding the Albian Gap. (c) The 2D PSDM seismic grid used in this study and its geographic location in relation to the 3D seismic surveys used in previous studies (Jackson et al., 2015a; Pichel et al., 2018; 2019b).

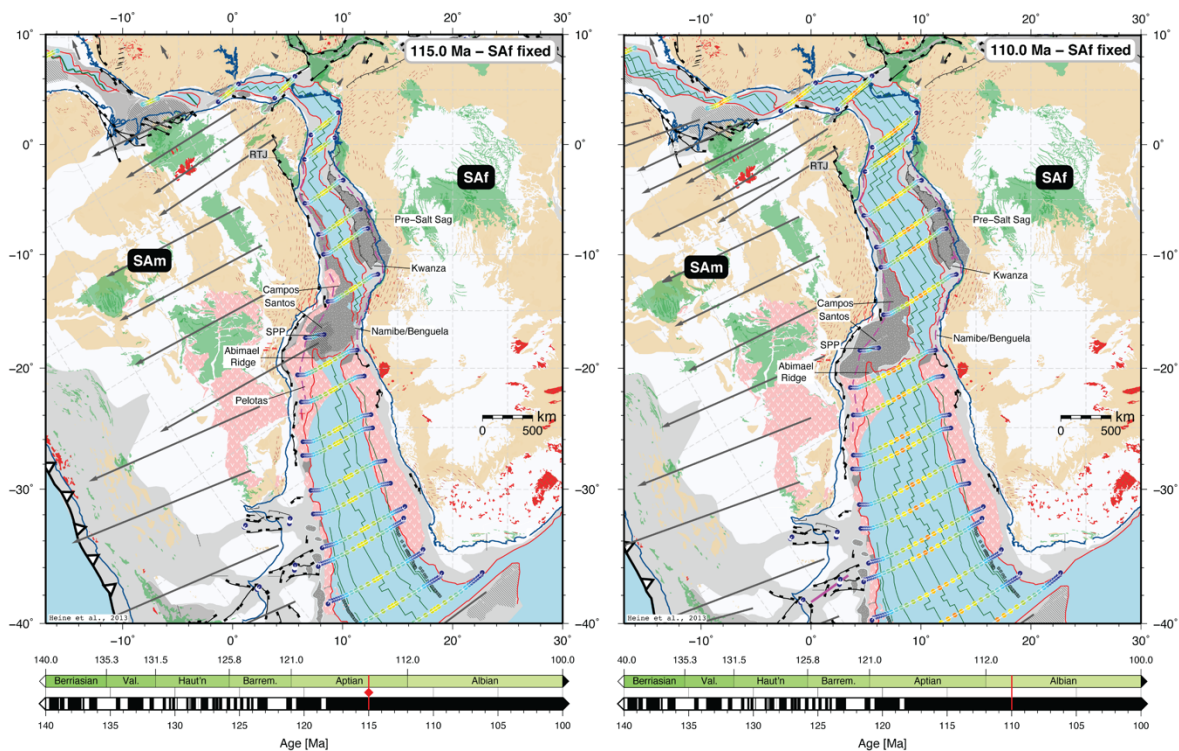


Figure 2: Plate Reconstruction at (a) mid-Aptian (115 Ma) and (b) early Albian (110 Ma) with Africa fixed in present-day coordinates (adapted from Heine et al., 2013) showing that breakup and seafloor spreading (in blue) had already initiated to the north (from NE Brazil down to the Espírito Santo Basin) and south (up to the Pelotas Basin and Abimaël Ridge) of the Santos Basin before the beginning of salt deposition. The Santos-Namibe/Benguela segments were the last ones to break up with extension becoming focused to the east of the Sao Paulo Plateau (SPP). By the early Albian, soon after salt deposition, the Santos Margin and its conjugate broke up after complete abandonment of the southern propagator coming from the Pelotas Basin. For the figures full caption, refer to Heine et al. (2013).



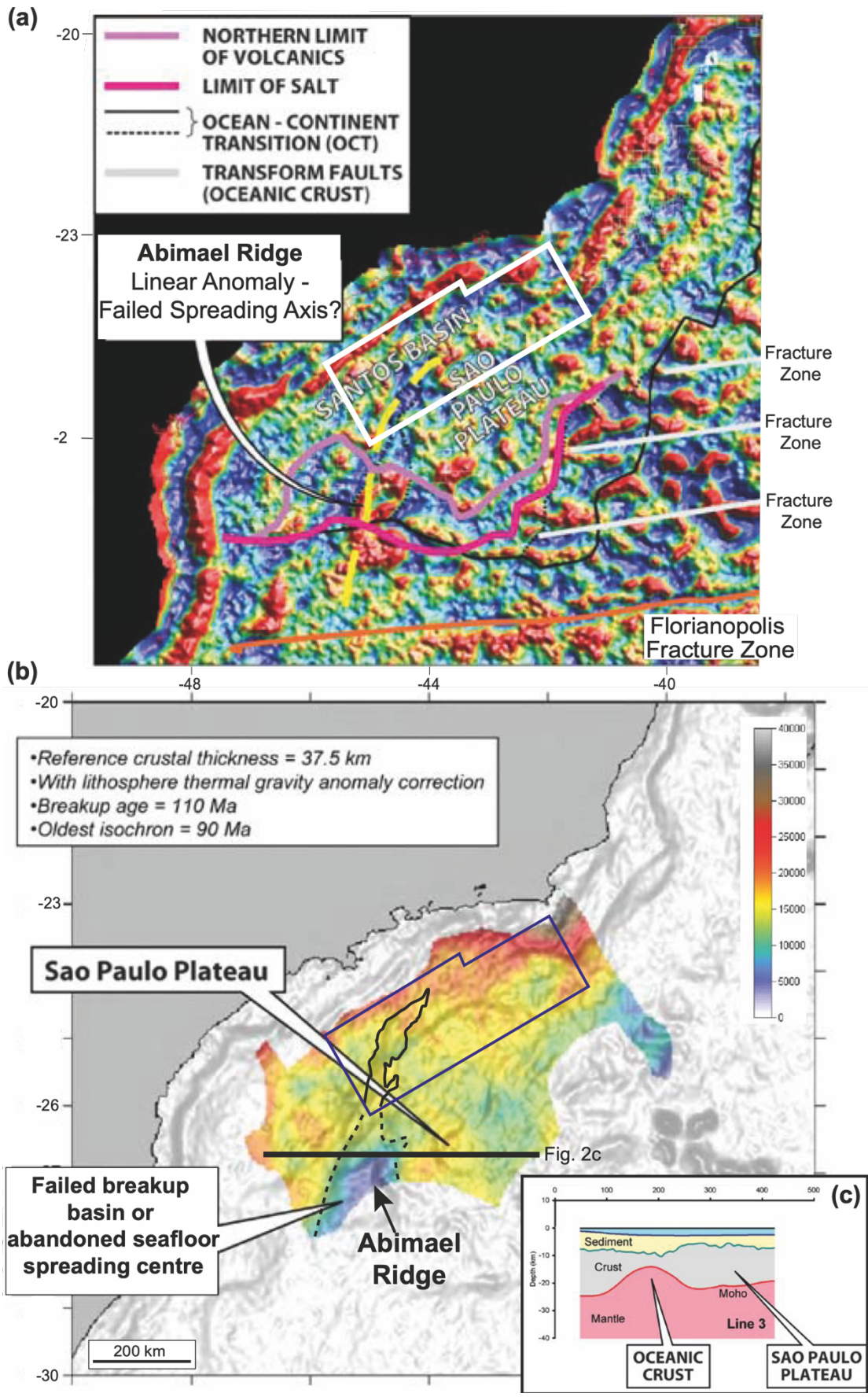


Figure 3: (a) Bouguer gravity anomaly map (200 km high-pass filter) of the central Santos Basin showing the linear feature with strong negative gravity anomaly (yellow dashed line), interpreted as a failed spreading-centre at the southern portion of our study-area (white polygon) (adapted from Scotchman et al. 2010). (b) Crustal basement thickness map derived from gravity inversion incorporating sediment thickness showing thinned continental crust underlying the São Paulo Plateau and oceanic crust at the Abimael Ridge (cf. Mohriak et al., 2008), which is located immediately adjacent and aligned with the Merluza Graben (black polygon) in our study-area (blue polygon) (adapted from Scotchman et al. 2010). Black line represents the crustal cross-section based on gravity-inversion data in (c), showing significantly thinner (< 5 km) crust and mantle upwelling underneath the failed spreading centre (adapted from Scotchman et al. 2010).

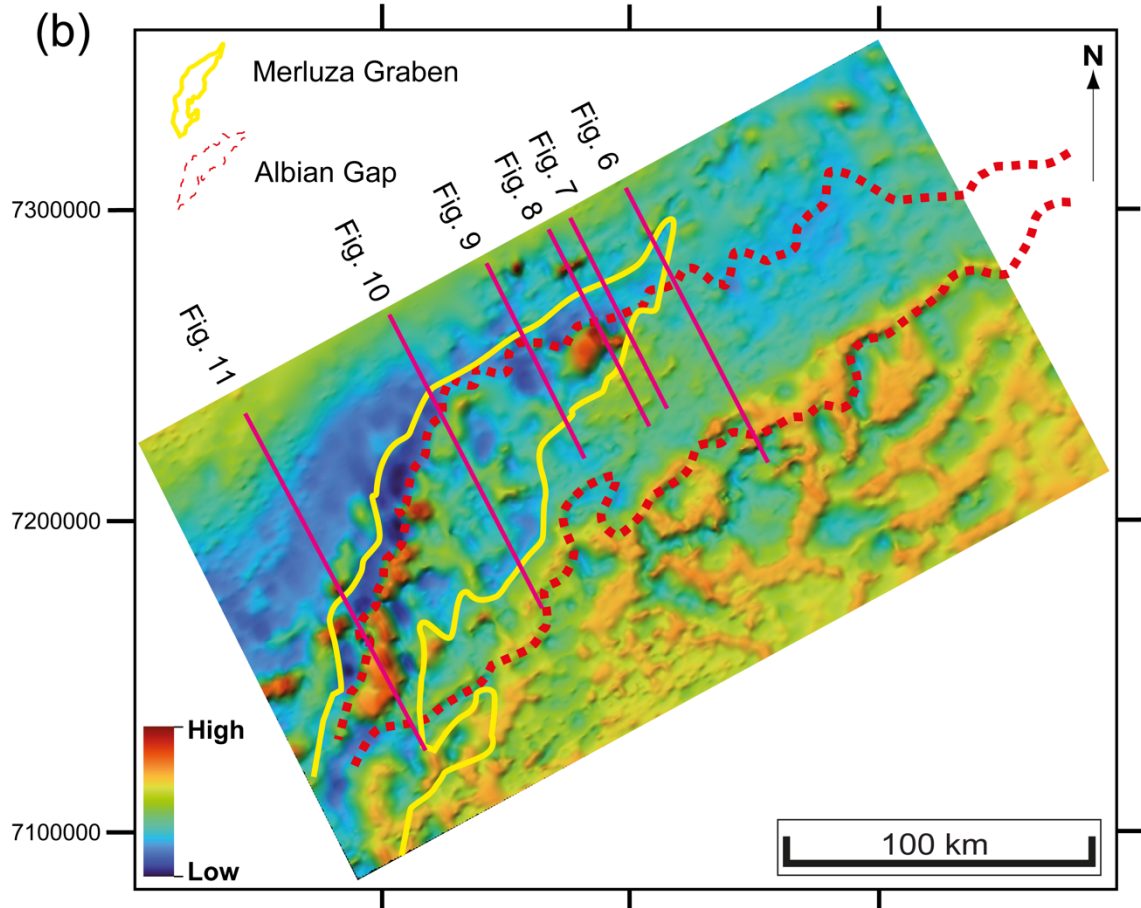
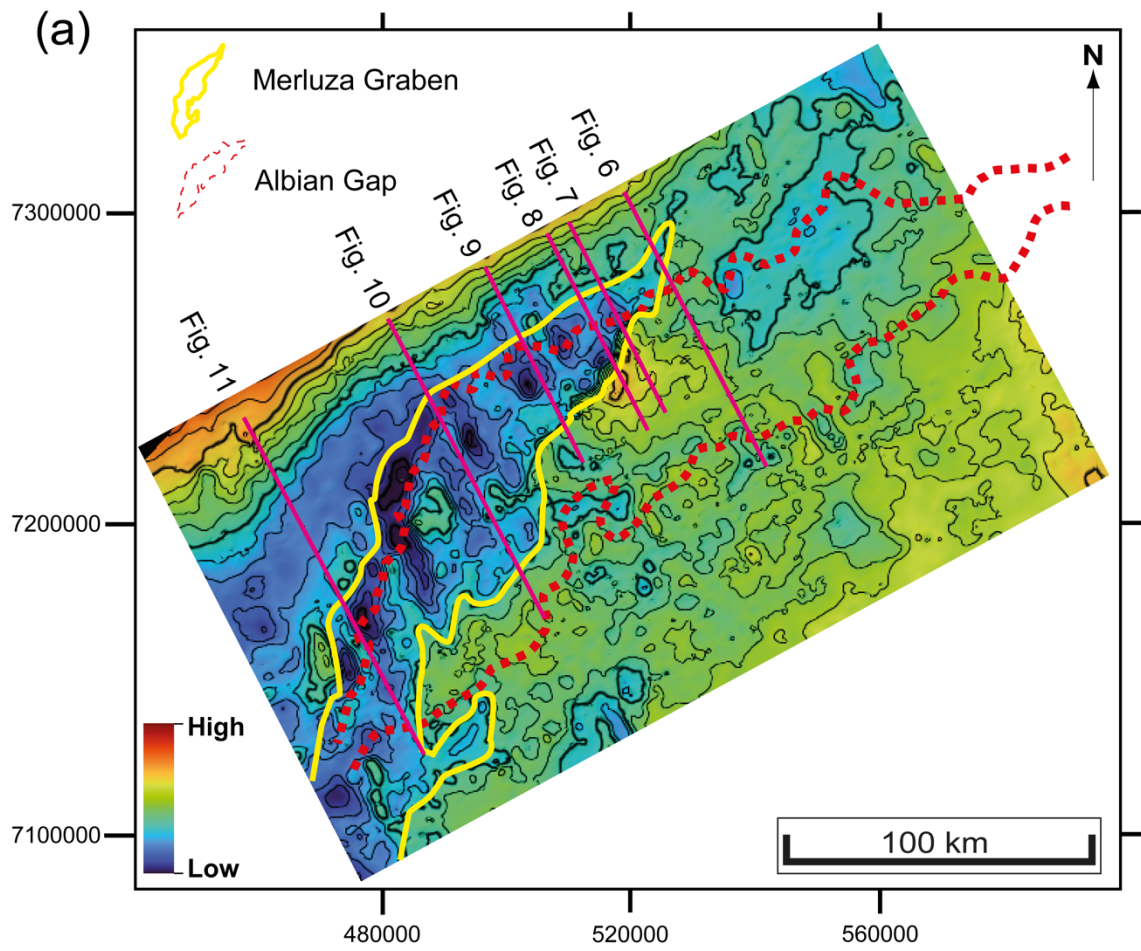


Figure 4: (a) Base-salt and (b) top-salt maps showing the outline of the Merluza Graben, which corresponds to a major and complex NNE-NE-oriented base-salt structural low with a few large diapirs, and the overlying Albian Gap, which is characterized by a structurally lower top-salt. Pink lines correspond to the seismic sections presented in the study.

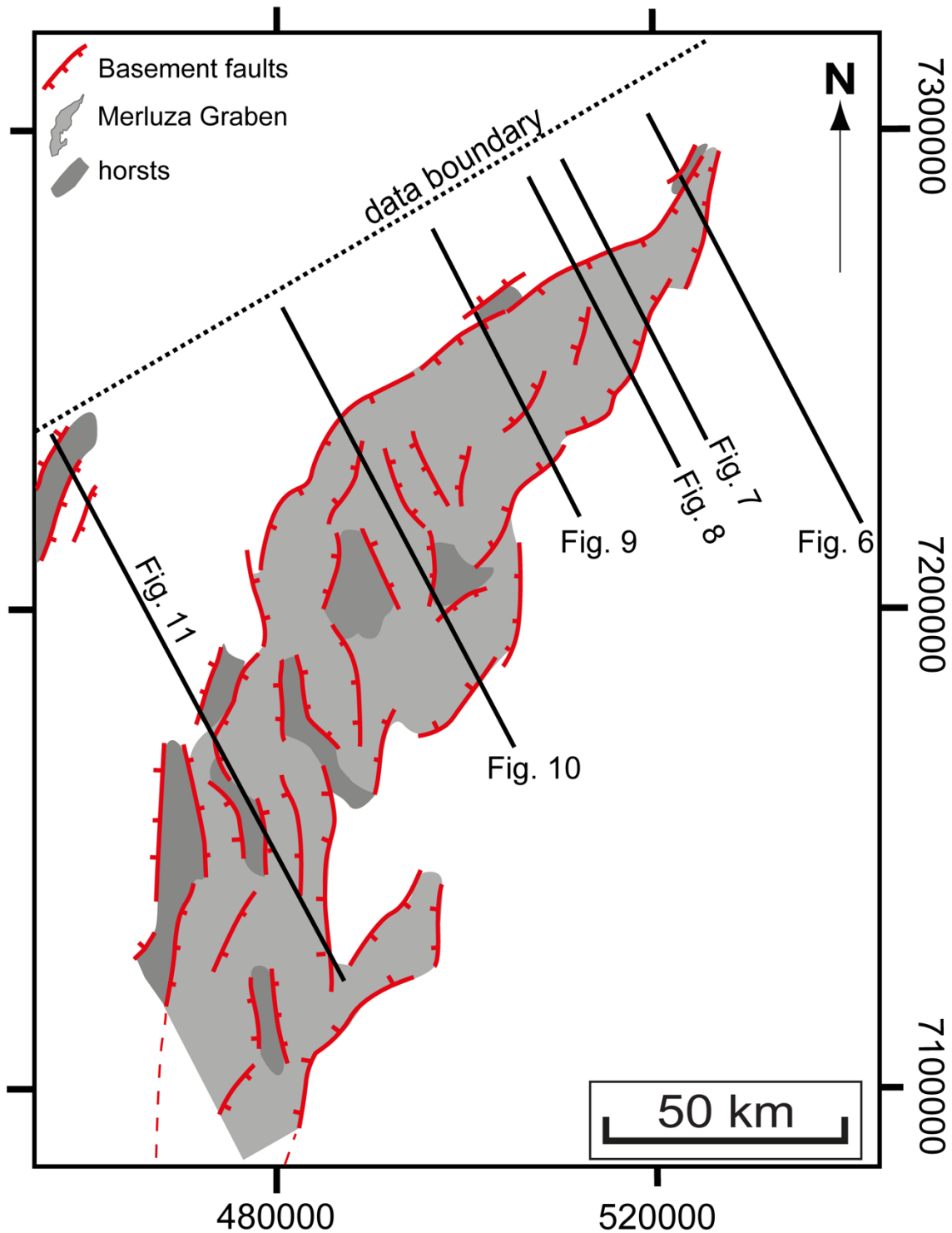


Figure 5: Simplified map showing the major base-salt structural elements associated with the Merluza



Graben. The graben is bound by a network of pre-salt rift-related faults that are broadly N-NNE oriented in the south and NE-oriented in the north. Smaller horsts and grabens also occur internally and marginally to the graben, being defined by a more complex network of faults, many of which oriented obliquely to the main structural grain.

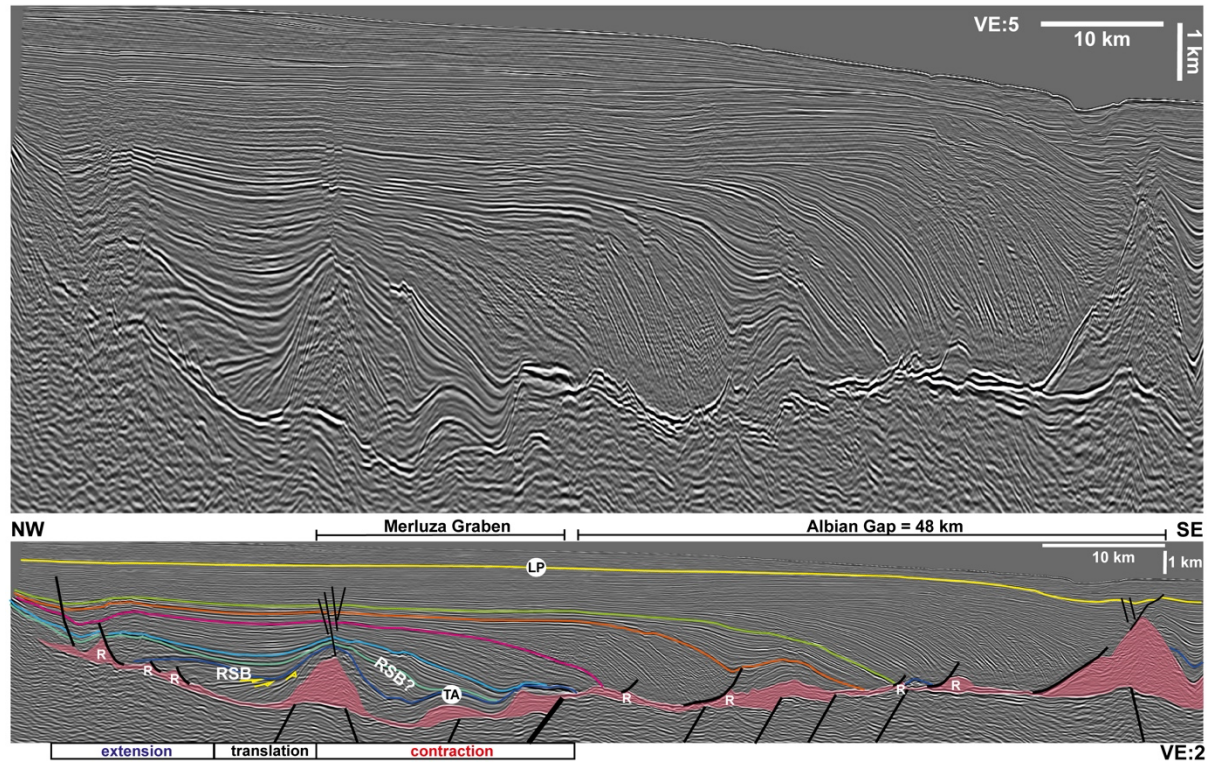


Figure 6: Seismic section intersecting the northern edge of the Merluza Graben and the adjacent Albian Gap. At this portion, the base-salt offset/relief of its basinward-bounding fault is smaller (c. 0.5 km) and salt-related deformation within and beyond the Merluza Gap are largely coupled with development of a large Late Cretaceous-Paleogene extension-expulsion rollover system. Salt structures are more variable within the Merluza Graben, with updip extensional rollers (R) passing downdip into a c. 5 km wide ramp-syncline basin (RSB) and onto a contractional salt anticlines at the updip and downdip edges of the graben, suggesting a strong influence of base-salt relief on salt flow. Earlier (Albian-LC2) structural domains are indicated in the bottom of the figure. Faults are in black, salt in transparent red and yellow arrows indicating erosional truncations of RSB strata. TA and LP refers to top Albian and late Paleogene unconformities, respectively. LC1-5 refer to key Late Cretaceous unconformities.

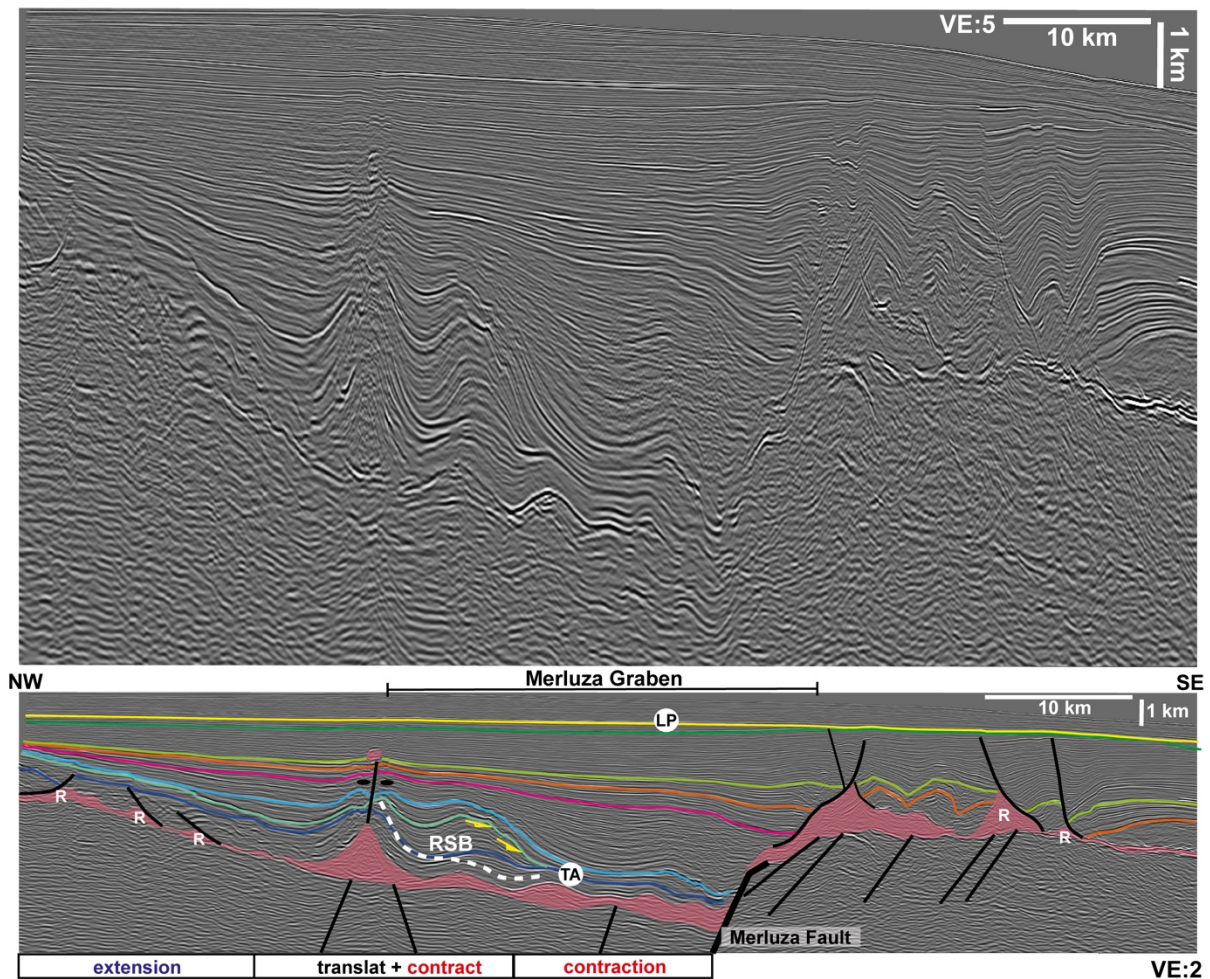


Figure 7: North section intersecting the Merluza Graben and its bounding Merluza Fault where its base-salt offset is c. 3 km. The section intersects part of the Albian Gap at the Merluza Fault footwall which is characterized by a series of extensional salt diapirs and salt rollers (R) defined by basinward-dipping listric faults. Due to its greater base-salt relief, salt deformation within the Merluza Graben is largely decoupled from its adjacent footwall resulting in marked strain partition within the Merluza Graben. This is characterized by updip extension (salt rollers, R), squeezed diapirs over its updip edge (base-salt horst), ramp-syncline basins (RSBs, onlap surfaces in white-dashed line above the basinward-dipping hangingwall and, adjacent the Merluza Fault, contractional anticlines overlain by an extensional rollover. Earlier (Albian-LC2) structural domains are indicated in the bottom of the figure. Faults are in black, salt in transparent red and yellow arrows indicating erosional truncations of RSB strata. TA and LP refers to top Albian and late Paleogene unconformities, respectively. LC1-5 refer to key Late Cretaceous unconformities.



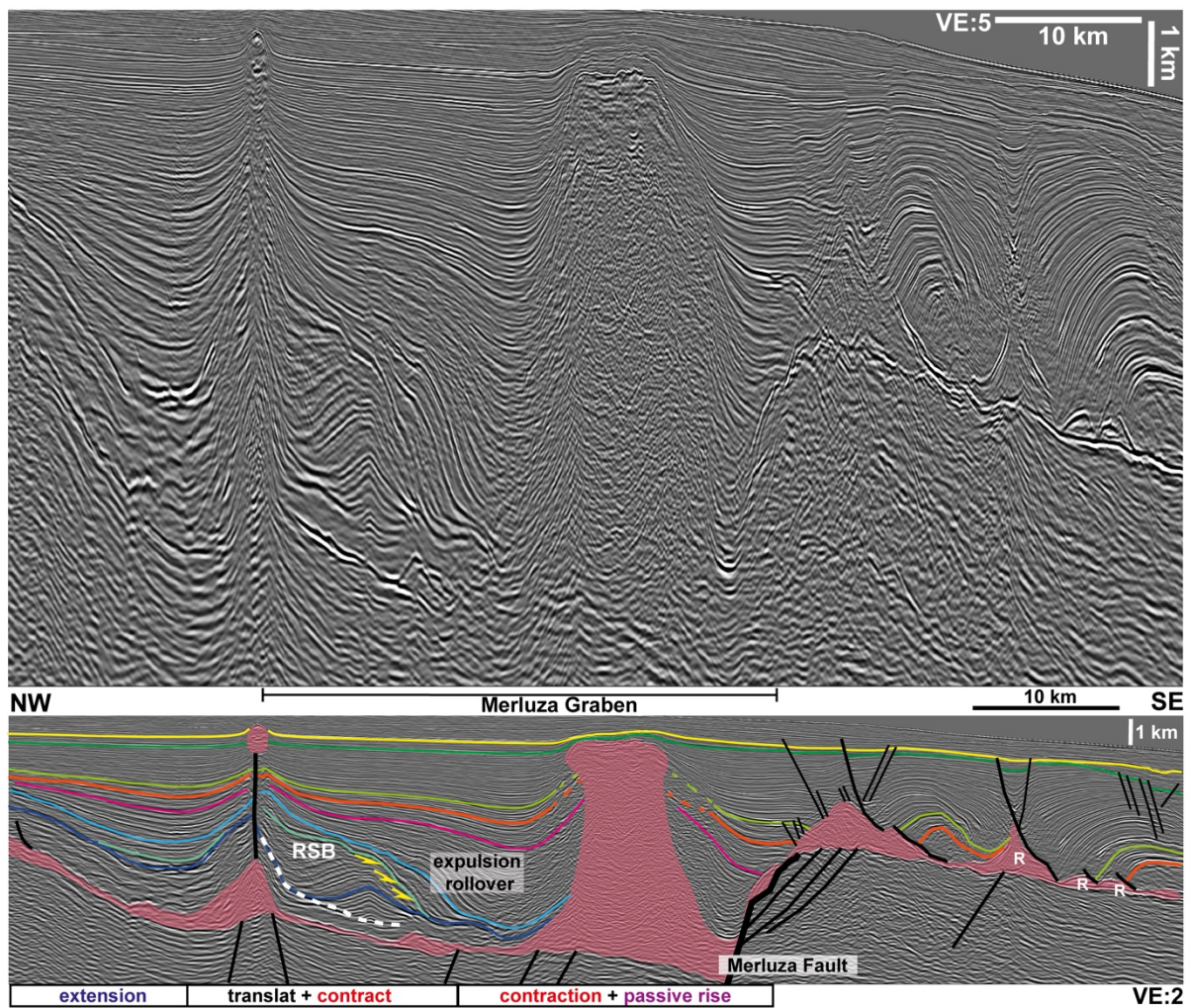


Figure 8: North section intersecting the Merluza Graben and its bounding Merluza Fault where its base-salt offset is greater 3.5 km. The section intersects part of the Albian Gap at the Merluza Fault footwall which is characterized by a series of extensional salt diapirs and salt rollers (R) defined by basinward-dipping listric faults. Due to its greater base-salt relief, salt deformation within the Merluza Graben is largely decoupled from its adjacent footwall resulting in marked strain partition within the Merluza Graben. This is characterized by updip extension (salt rollers, R), squeezed diapirs over its updip edge (base-salt horst), ramp-syncline basins (RSBs, onlap surfaces in white-dashed line) and later expulsion rollover above the basinward-dipping hangingwall and, adjacent the Merluza Fault, a large salt stock. Earlier (Albian-LC2) structural domains are indicated in the bottom of the figure. Faults are in black, salt in transparent red and yellow arrows indicating erosional truncations of RSB strata. TA and LP refers to top Albian and late Paleogene unconformities, respectively. LC1-5 refer to key Late Cretaceous unconformities.



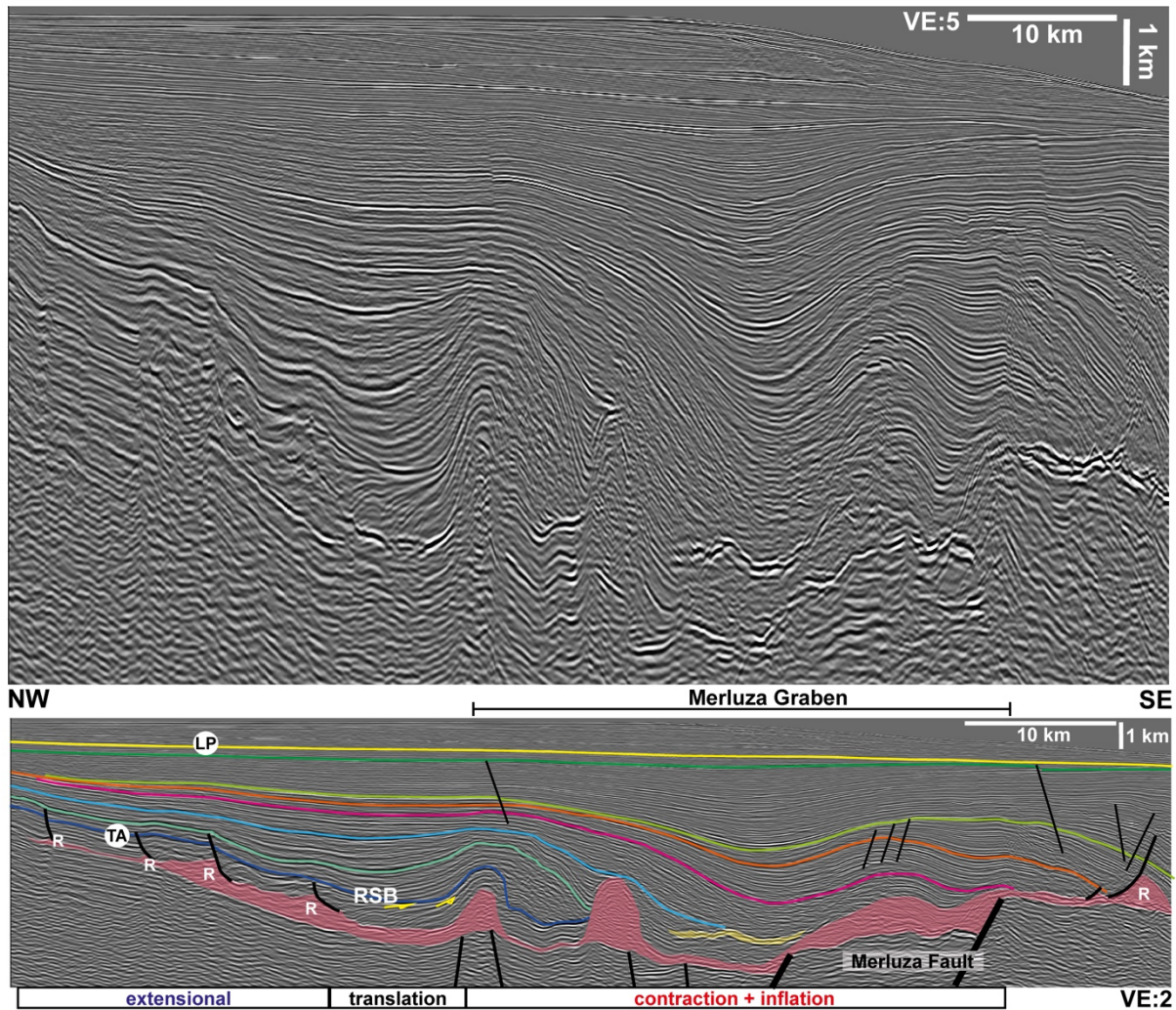


Figure 9: North-central section showing structural variability and transition from early (Albian-LC1) updip extension (salt rollers, R), intermediate translation (RSB) and downdip shortening (salt anticlines) at the edges of the Merluza Graben as well as above its internal faults. Subsequent deformation (LC2 onwards) is characterized by sediment progradation and a switch from translation to expulsion-driven basinward salt flow, which is initially buttressed against the Merluza Fault during LC2-3. Earlier (Albian-LC2) structural domains are indicated in the bottom of the figure. Faults are in black, salt in transparent, red and yellow arrows indicating erosional truncations of RSB strata. TA and LP refers to top Albian and late Paleogene unconformities, respectively. LC1-5 refer to key Late Cretaceous unconformities.



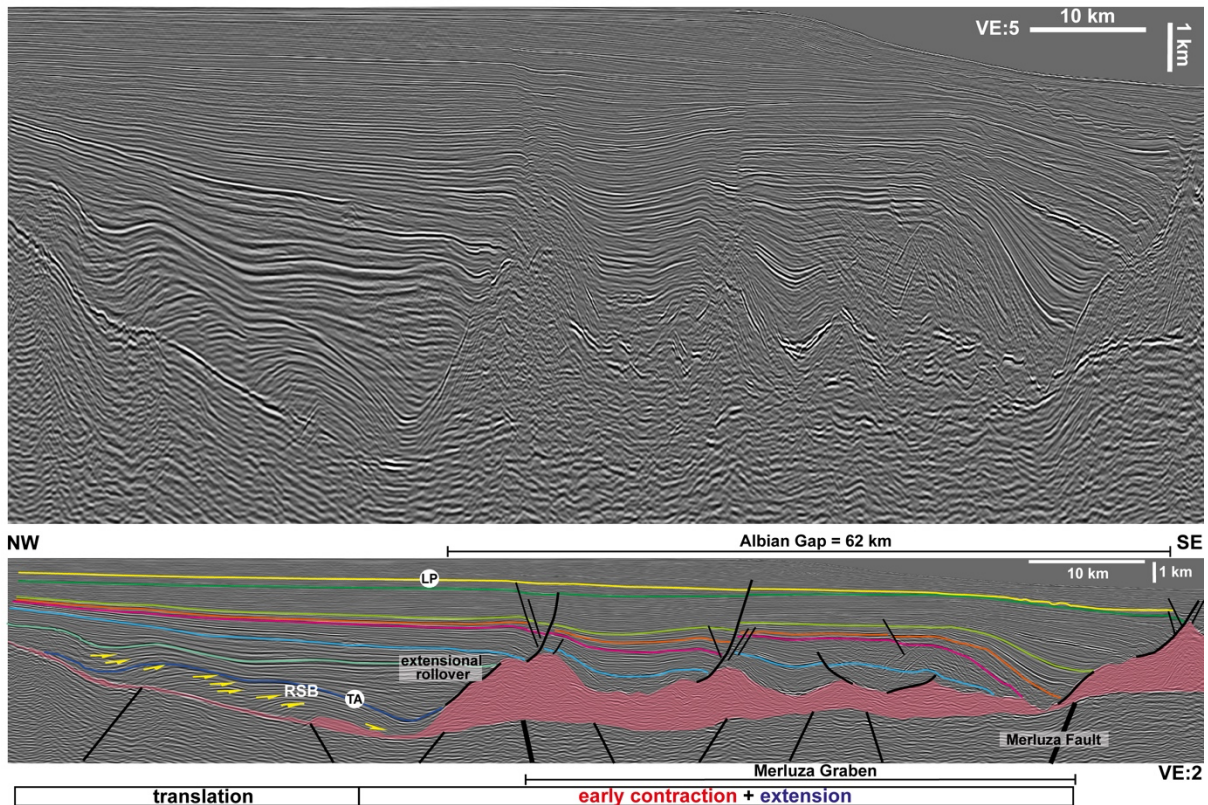


Figure 10: South-central section showing a large RSB section forming over a wide basinward-dipping base-salt segment updip of the Merluza Graben, transitioning up and basinward into a LC1-2 extensional rollover. In the Merluza Graben, a lack of Albian-LC1 strata indicates early salt inflation and/or passive diapirism and subsequent extension and salt expulsion due to progradation of LC2-5 strata. In this portion of the study-area, the Albian Gap is largely controlled by the original salt distribution and deformation styles within the Merluza Graben as the two structures overlap in space. Earlier (Albian-LC2) structural domains are indicated in the bottom of the figure. Faults are in black, salt in transparent red and yellow arrows indicating erosional truncations of RSB strata. TA and LP refers to top Albian and late Paleogene unconformities, respectively. LC1-5 refer to key Late Cretaceous unconformities.

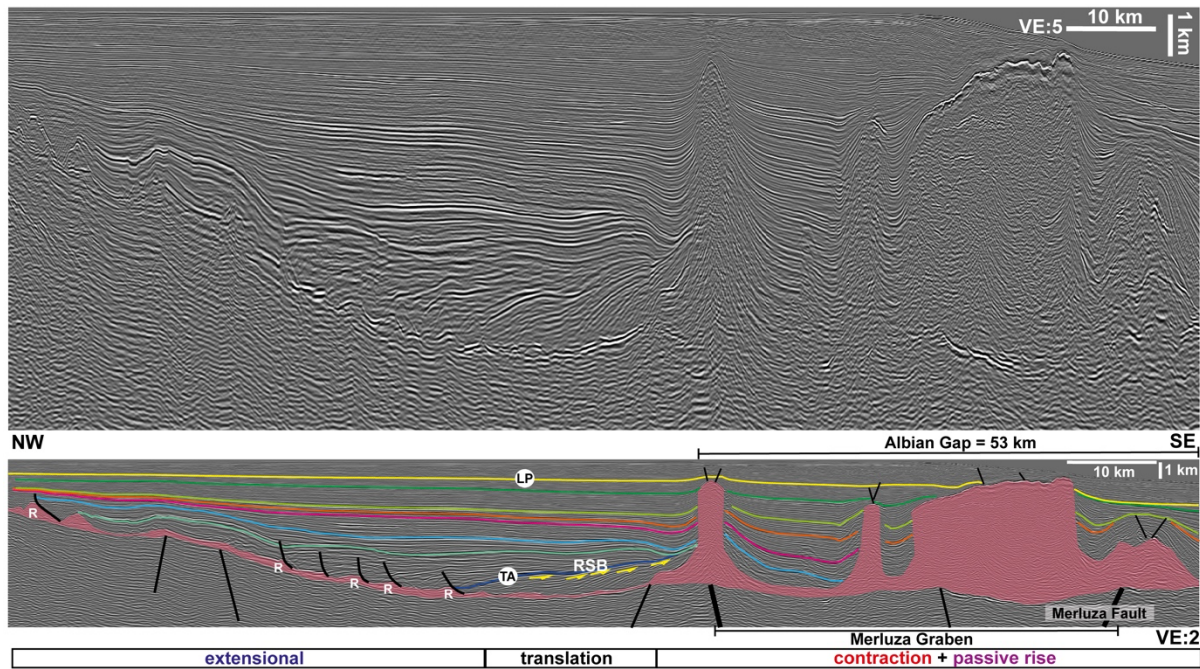


Figure 11: South section illustrating the transition for the updip extensional domain characterized by a series of small Albian-LC1 salt rollers (R) transitioning basinward into a large RSB and a tall, squeezed diapir over the updip edge of the Merluza Graben. In the Merluza Graben, the style of deformation is characterized by thick minibasins and 4-5 km tall and up to 10 km wide salt walls indicating a style of deformation largely characterized by load-driven subsidence and diapirism with minor late shortening. In this portion of the study-area, the Albian Gap is largely controlled by the original salt distribution and deformation styles within the Merluza Graben as the two structures overlap in space. Earlier (Albian-LC2) structural domains are indicated in the bottom of the figure. Faults are in black, salt in transparent, red and yellow arrows indicating erosional truncations of RSB strata. TA and LP refers to top Albian and late Paleogene unconformities, respectively. LC1-5 refer to key Late Cretaceous unconformities.

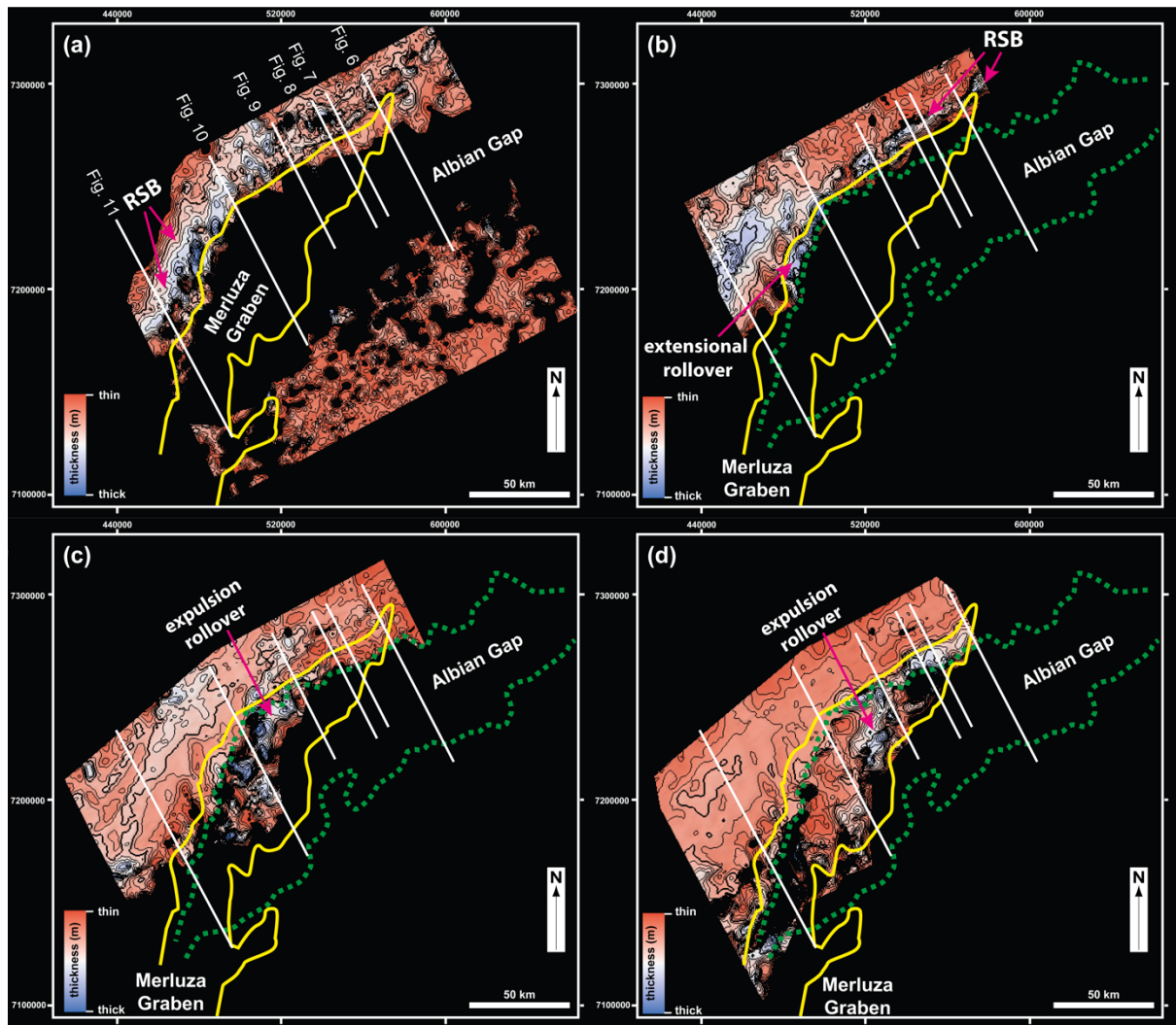


Figure 12: Thickness maps of (a) Albian, (b) LC1, (c) LC2 and (d) LC3, the main stratigraphic intervals influenced by base-salt architecture and offset associated with the Merluza Graben, outlined in yellow. Albian Gap is outlined in green and seismic profiles used in white. These maps combined show a clear pattern of basinward shift of depocentres (thickest intervals in blue-white colours) through time. Depocentres formed during the earliest intervals (Albian-LC2) were more variable and more influenced by the geometry of the Merluza Graben. During Albian and LC1, linear depocentres at the updip edge of the Merluza Graben correspond to RSBs, the ones further updip to extension rollovers (see figs. 5-8). During LC3, thickness changes were less pronounced and confined predominantly to expulsion rollovers surrounding inflated salt diapirs and/or anticlines at the basinward edge of the Merluza Graben.



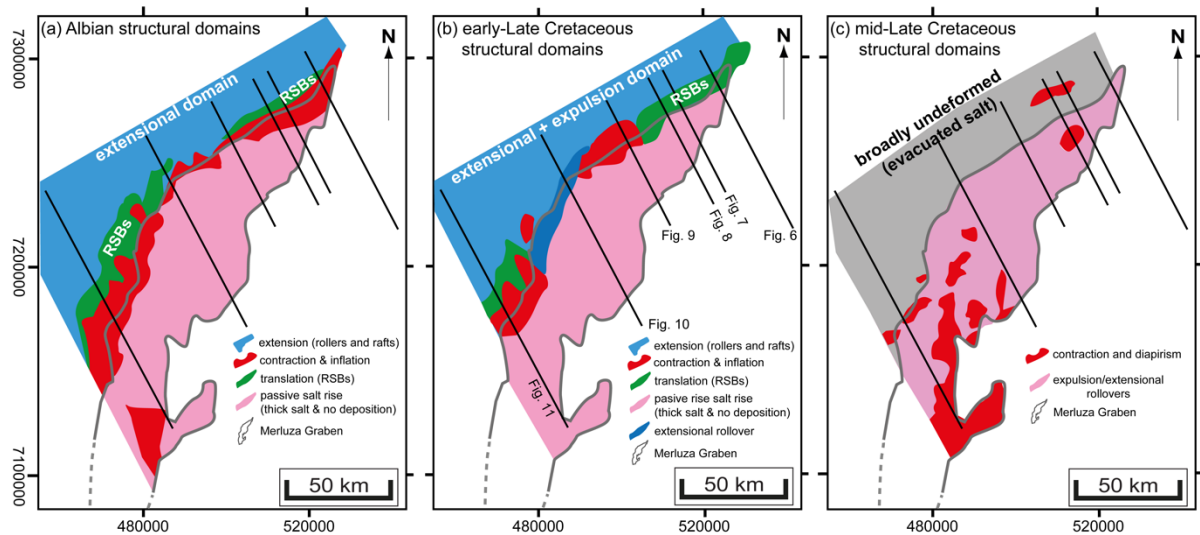


Figure 13: Simplified structural maps based on structural and thickness maps of figures 11 and 12 for the post-salt intervals more significantly influenced by the Merluza Graben: (a) Albian, (b) LC1, (c) LC3. Earliest intervals (Albian and LC1) are significantly more variable as a result of sediment progradation and translation above the complex updip edge of the Merluza Graben. This resulted in updip extension (salt rollers and extensional rollovers), intermediate translation (RSBs) and downdip contraction at the updip edge of the Merluza Graben and passive diapirism further downdip within the graben. During the mid-Late Cretaceous (LC2), updip extension and basinward translation ceased due to near-complete evacuation of updip salt and buttressing of basinward salt flow against the bounding Merluza Fault. This resulted in the development of expulsion-extensional rollovers within most of the graben, inflation and/or contraction to the south and salt diapirism near the basinward edge of the graben.

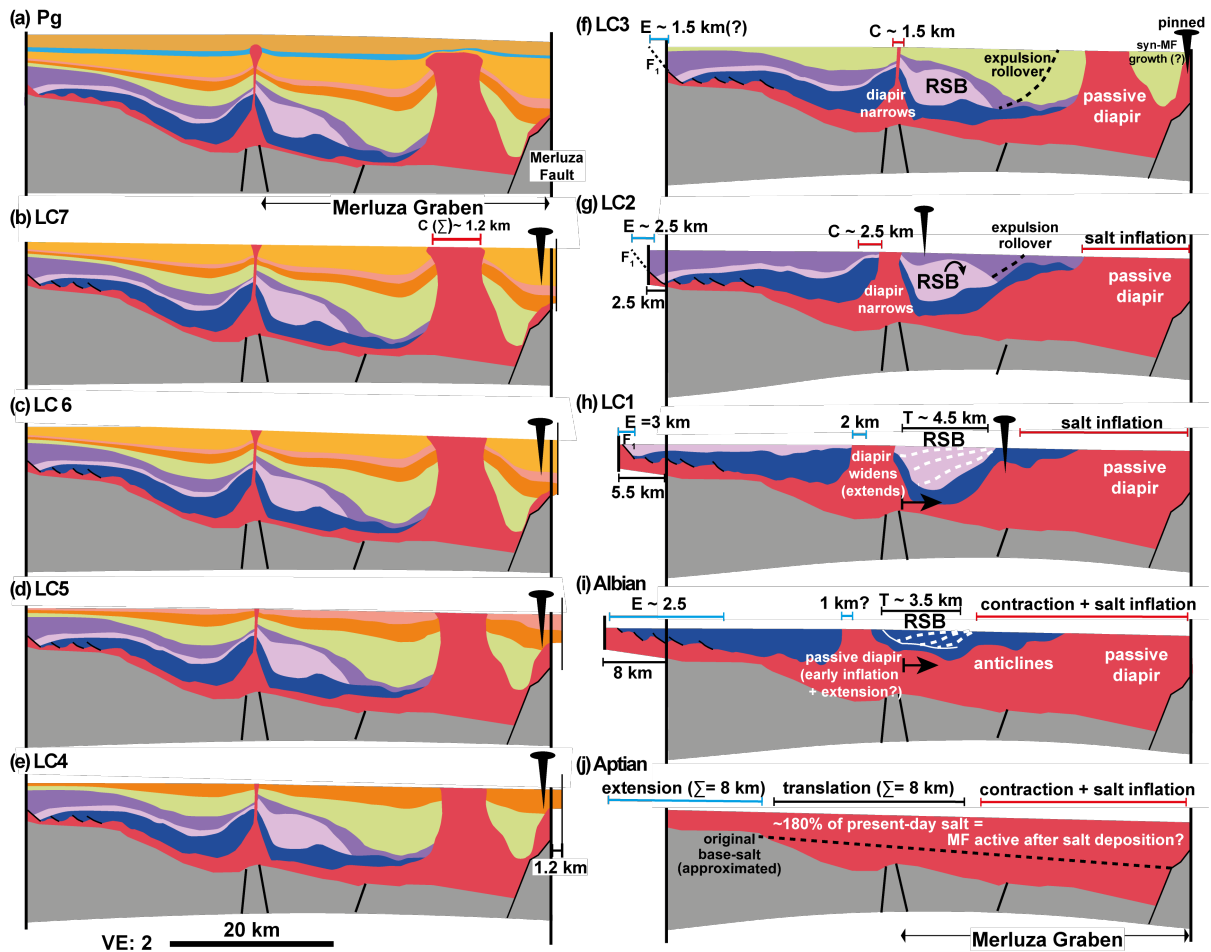


Figure 14: Restoration of Section A, which corresponds to the seismic section in Fig. 6b. The restoration incorporates decompaction with flexural isostasy and unfolding with simple shear and move-on-fault algorithms. Pins indicate the position where translation ceased due to depletion of the salt interval or buttressing against base-salt highs at each time-step. Basement in grey, salt in red and post-salt horizons follow their respective colour from seismic profiles (see Fig. 6).

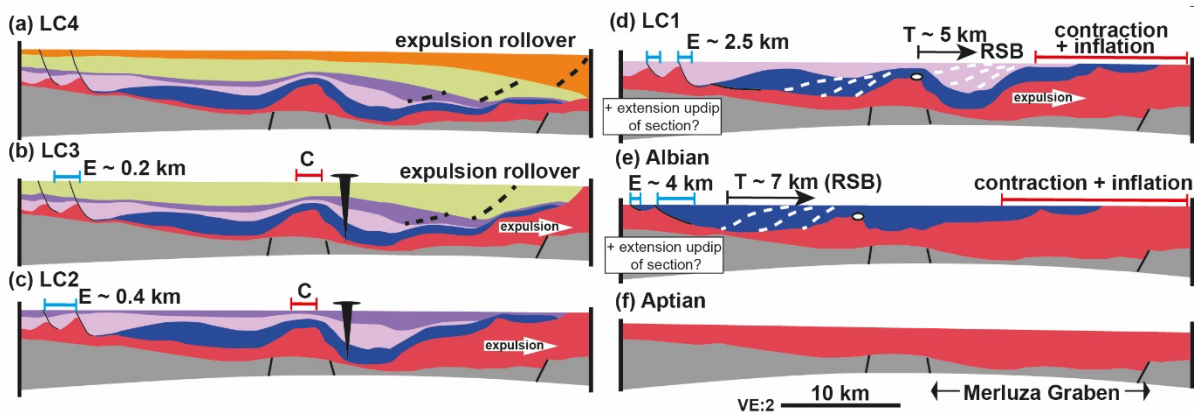


Figure 15: Restoration of Section B, which corresponds to the seismic section in Fig. 5. The restoration incorporates decompaction with flexural isostasy and unfolding with simple shear and move-on-fault

algorithms. Temporary pins indicate the position where overburden translation ceased due to depletion and/or welding of the salt interval at each time-step. Basement in grey, salt in red and post-salt horizons follow their respective colour from seismic profiles (see Fig. 5).

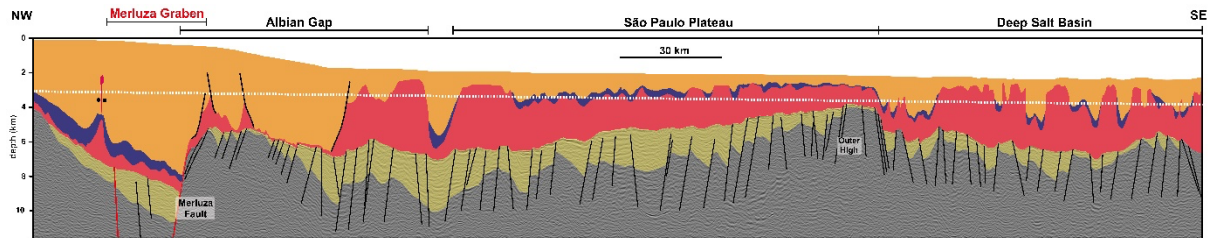
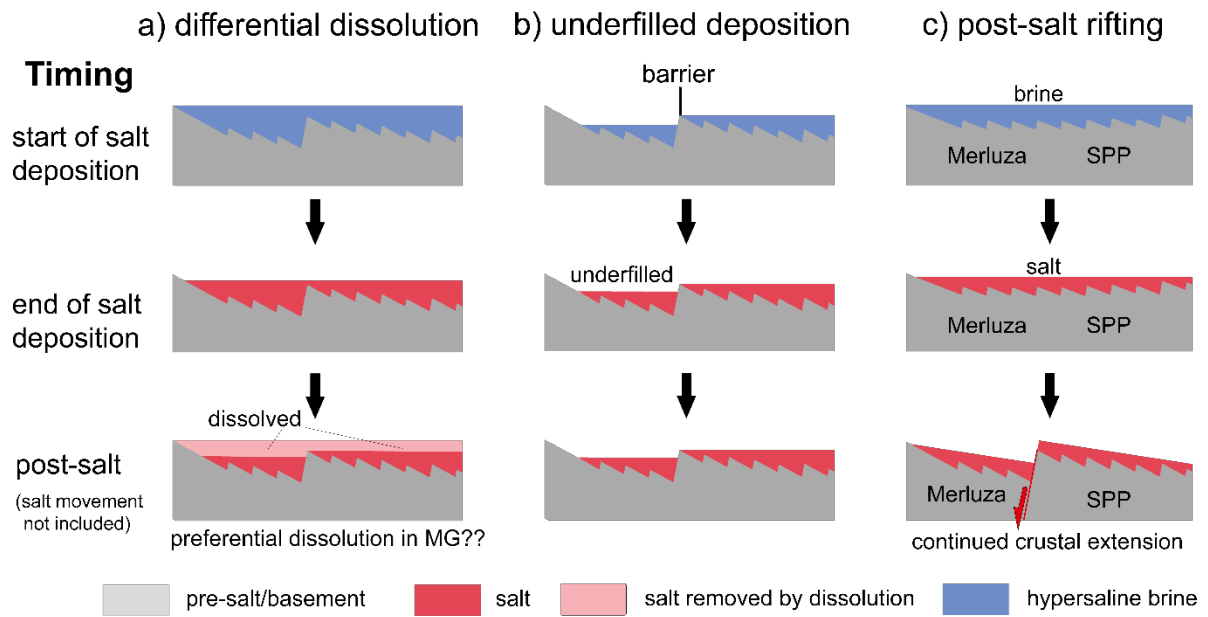


Figure 16: Dip-oriented seismic transect illustrating the pre-salt basement, syn-rift (yellow), and salt (red) structural architecture in the Santos Basin and its main structural provinces: the Merluza Graben, the Albian Gap, the São Paulo Plateau and the Deep Salt Basin. Note the significantly more variable and rugose base-salt relief around the Merluza Graben and Deep Salt Basin in contrast with the more subtle base-salt relief in the São Paulo Plateau. Also note the contrasting salt thickness and structural styles between the domains. The Merluza Graben and Albian Gap are characterized by a significantly thinner salt, thicker overburden and dominantly extensional deformation as opposed to thicker and inflated salt with passive diapirs and salt-cored folds on the São Paulo Plateau, passing downdip into large salt walls and thick minibasins in the Deep Salt Basin. The white dashed-line is an inferred regional datum representing the minimum depositional top-salt elevation relative to its base (i.e., depositional salt thickness) that would allow the salt layer to be connected across the basin. For that, the Merluza Graben would have a maximum salt thickness of c. 5 km, which is largely inconsistent with seismic observations and thus indicates that the Merluza Fault was active after salt deposition. Faults are in black, Albian in blue and post-Albian strata in yellow. The Merluza Graben bounding faults are in red.

## ALTERNATIVE MODELS



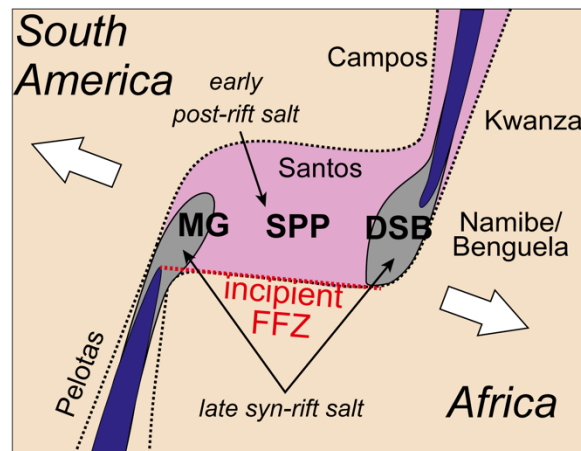
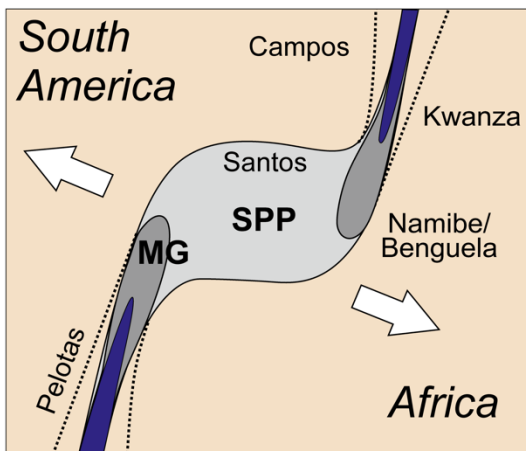
*Fig. 17: Alternative models explaining the discrepancy between salt and the pre-salt Merluza Graben area by the end of salt deposition (late Aptian). (a) differential dissolution over the Merluza Graben, (b) underfilling of the Merluza Graben, (c) post-salt rifting and Merluza Fault activity.*

### a) Barremian-early Aptian:

- focussed rifting ahead of rift propagators,
- distributed deformation between rift propagators - development of SPP

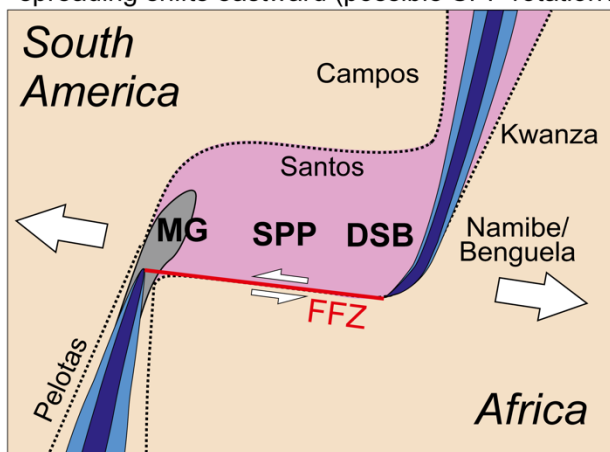
### b) late Aptian-early Albian

- distributed rifting ceased, deformation focused on rift propagators as they develop a link (FFZ),
- salt deposition in areas not actively rifting (**post-rift salt**) with exception of **MG** and **DSB** (**syn-rift salt**)



### c) late Albian-Cenomanian

- change of rifting direction (cf. Heine et al., 2013),
- oceanic spreading connected through FFZ,
- **prolonged extension** over **MG** as oceanic spreading shifts eastward (possible SPP rotation?)



#### Legend

- distributed rifting
- focussed rifting
- inactive rifting
- active spreading
- inactive spreading (oceanic crust)
- salt basin

#### Santos Structural Provinces

- |                              |                                     |
|------------------------------|-------------------------------------|
| <b>MG</b> Merluza Graben     | <b>DSB</b> Deep Salt Basin          |
| <b>SPP</b> São Paulo Plateau | <b>FFZ</b> Florianópolis Fault Zone |

Figure 18: Schematic evolutionary model of the 3D linkage between two propagating spreading centres and its influence on the rift-related activity and architecture as well as salt deposition in the Santos Basin and adjacent salt basin in the South Atlantic. The São Paulo Plateau formed prior to salt deposition due to distributed rifting between the two laterally overlapping spreading centres during Barremian-early Aptian times (a). Salt was deposited after rifting ceased in the São Paulo Plateau but during ongoing rifting in the Deep Salt Basin and Merluza Graben, which were both located ahead of the southern and northern propagators, respectively. The subsequent abortion of the southern spreading centre and consequent shift of spreading eastward, towards Africa, resulted in a significantly wider salt basin in Santos than elsewhere in the South Atlantic and insignificant salt in the conjugate



*Namibe Basin. Rifting continued locally in the Merluza Graben as a result of collapse of the aborted southern spreading centre during and soon after the rift jump as the area was characterized by highly-stretched and weakened crust and was, consequently, more prone to failure than the adjacent structural domains.*

## **References**

Adam, J., & Krézsek, C. (2012). Basin-scale salt tectonic processes of the Laurentian Basin, Eastern Canada: insights from integrated regional 2D seismic interpretation and 4D physical experiments. *Geological Society, London, Special Publications*, 363(1), 331-360.

Allen, H., Jackson, C. A. L., & Fraser, A. J. (2016). Gravity-driven deformation of a youthful saline giant: the interplay between gliding and spreading in the Messinian basins of the Eastern Mediterranean. *Petroleum Geoscience*, 22(4), 340-356.

Augustin, N., Devey, C. W., van der Zwan, F. M., Feldens, P., Tominaga, M., Bantan, R. A., & Kwasnitschka, T. (2014). The rifting to spreading transition in the Red Sea. *Earth and Planetary Science Letters*, 395, 217-230.

Benoit, I., Nicolas, S., & Serrano, O. (2020). Role of structural inheritance and salt tectonics in the formation of pseudosymmetric continental rifts on the European margin of the hyperextended Mauléon basin (Early Cretaceous Arzacq and Tartas Basins). *Marine and Petroleum Geology*, 118, 104395.

Blaich, O. A., Faleide, J. I., & Tsikalas, F. (2011). Crustal breakup and continent-ocean transition at South Atlantic conjugate margins. *Journal of Geophysical Research: Solid Earth*, 116(B1).

Brown, A. R. (2011). Interpretation of three-dimensional seismic data. Society of Exploration Geophysicists and American Association of Petroleum Geologists.

Burrell, L., & Teixell, A. (2021). Contractional salt tectonics and role of pre-existing diapiric structures in the South Pyrenean foreland fold-and-thrust belt (Montsec and Serres Marginals). *Journal of the Geological Society*.

Célini, N., Callot, J. P., Ringenbach, J. C., & Graham, R. (2020). Jurassic Salt Tectonics in the SW Sub-Alpine Fold-and-Thrust Belt. *Tectonics*, 39(10).

Cobbold, P. R., Szatmari, P., Demercian, L. S., Coelho, D., Rossello, E. A. (1995). Seismic and experimental evidence for thin-skinned horizontal shortening by convergent radial gliding on evaporites, deep-water Santos Basin, Brazil, in: Jackson, M. P. A., Roberts, D. G., Snelson, S. (eds) Salt tectonics: a global perspective. AAPG Memoir 65, 305-321.

Curry, M. A., Peel, F. J., Hudec, M. R., & Norton, I. O. (2018). Extensional models for the development of passive-margin salt basins, with application to the Gulf of Mexico. *Basin Research*, 30(6), 1180-1199.

Davison, I. (2005). Central Atlantic margin basins of North West Africa: geology and hydrocarbon potential (Morocco to Guinea). *Journal of African Earth Sciences*, 43(1-3), 254-274.

Davison, I., Anderson, L., Nuttall, P. (2012). Salt deposition, loading and gravity drainage in the Campos and Santos salt basins. *Geological Society of London Special Publications*, 363(1), 159-174.

Decarlis, A., Maino, M., Dallagiovanna, G., Lualdi, A., Masini, E., Seno, S., & Toscani, G. (2014). Salt tectonics in the SW Alps (Italy–France): From rifting to the inversion of the European continental margin in a context of oblique convergence. *Tectonophysics*, 636, 293-314.

Demercian, S., Szatmari, P., Cobbold, P. R. (1993). Style and pattern of salt diapirs due to thin-skinned gravitational gliding, Campos and Santos basins, offshore Brazil. *Tectonophysics*, 228(3-4), 393-433.

Deptuck, M. E., & Kendall, K. L. (2017). A review of Mesozoic-Cenozoic salt tectonics along the Scotian margin, eastern Canada. In *Permo-Triassic Salt Provinces of Europe, North Africa and the Atlantic Margins* (pp. 287-312). Elsevier.

Dooley, T. P., Hudec, M. R., Carruthers, D., Jackson, M. P., Luo, G. (2016). The effects of base-salt relief on salt flow and suprasalt deformation patterns—Part 1: Flow across simple steps in the base of salt. *Interpretation*, 5(1), SD1-SD23.

Dooley, T. P., Hudec, M. R. (2016). The effects of base-salt relief on salt flow and suprasalt deformation patterns—Part 2: Application to the eastern Gulf of Mexico. *Interpretation*, 5(1), SD25-SD38.

Dooley, T. P., Hudec, M. R., Pichel, L. M., Jackson, M. P. (2018). The impact of base-salt relief on salt flow and suprasalt deformation patterns at the autochthonous, paraautochthonous and allochthonous level: insights from physical models. *Geological Society, London, Special Publications*, 476, SP476-13.

Evans, S. L., & Jackson, C. A. L. (2020). Base-salt relief controls salt-related deformation in the Outer Kwanza Basin, offshore Angola. *Basin Research*, 32(4), 668-687.

Ferrer, O., Roca, E., Vendeville, B.C. (2014). The role of salt layers in the hangingwall deformation of kinked-planar extensional faults: Insights from 3D analogue models and comparison with the Parentis Basin. *Tectonophysics*, 636, 338-350.

Ford, M., & Vergés, J. (2021). Evolution of a salt-rich transtensional rifted margin, eastern North Pyrenees, France. *Journal of the Geological Society*, 178(1).

Fiduk, J. C., & Rowan, M. G. (2012). Analysis of folding and deformation within layered evaporites in Blocks BM-S-8 &-9, Santos Basin, Brazil. *Geological Society, London, Special Publications*, 363(1), 471-487.

Garcia, S. F., Letouzey, J., Rudkiewicz, J. L., Danderfer Filho, A., & de Lamotte, D. F. (2012). Structural modeling based on sequential restoration of gravitational salt deformation in the Santos Basin (Brazil). *Marine and Petroleum Geology*, 35(1), 337-353.

Giles, K. A., & Rowan, M. G. (2012). Concepts in halokinetic-sequence deformation and stratigraphy. Geological Society, London, Special Publications, 363(1), 7-31.

Garcia, S. F., Letouzey, J., Rudkiewicz, J. L., Danderfer Filho, A., & de Lamotte, D. F. (2012). Structural modeling based on sequential restoration of gravitational salt deformation in the Santos Basin (Brazil). *Marine and Petroleum Geology*, 35(1), 337-353.

Guerra, M. C., Underhill, J. R. (2012). Role of halokinesis in controlling structural styles and sediment dispersal in the Santos Basin, offshore Brazil. Geological Society, London, Special Publications, 363(1), 175-206.

Gomes, P. O., Kilsdonk, B., Minken, J., Grow, T., & Barragan, R. (2009). The outer high of the Santos Basin, Southern São Paulo Plateau, Brazil: pre-salt exploration outbreak, paleogeographic setting, and evolution of the syn-rift structures. In AAPG International Conference and Exhibition (pp. 15-18).

Hadler-Jacobsen, F., Groth, A., Hearn, R.E., and Liestøl, F.M. (2010), Controls on and expressions of submarine fan genesis within a high accommodation margin setting, Santos Basin, Brazil—A high-resolution seismic stratigraphic and geomorphic case study, in Wood, L.J., Simo, T.T., and Rosen, N.C., eds., *Seismic Imaging of Depositional and Geomorphic Systems: Gulf Coast Section Society for Sedimentary Geology Foundation Annual Bob F. Perkins Research Conference Proceedings*, v. 30, p. 572–615.

Heine, C., Zoethout, J., & Müller, R. D. (2013). Kinematics of the South Atlantic rift. *Solid Earth*, 4(2), 215-253.

Hudec, M. R., Jackson, M. P. A. (2004). Regional restoration across the Kwanza Basin, Angola: Salt tectonics triggered by repeated uplift of a metastable passive margin. AAPG bulletin, 88(7), 971-990.

Hudec, M. R., Norton, I. O., Jackson, M. P., & Peel, F. J. (2013). Jurassic evolution of the Gulf of Mexico salt basin. Gulf of Mexico Jurassic Evolution. AAPG bulletin, 97(10), 1683-1710.

Hudec, M. R., & Norton, I. O. (2019). Upper Jurassic structure and evolution of the Yucatán and Campeche subbasins, southern Gulf of Mexico. AAPG Bulletin, 103(5), 1133-1151.

Hudec, M. R., Dooley, T. P., Peel, F. J., & Soto, J. I. (2019). Controls on the evolution of passive-margin salt basins: Structure and evolution of the Salina del Bravo region, northeastern Mexico. Geological Society of America Bulletin.

Huisman, R., & Beaumont, C. (2011). Depth-dependent extension, two-stage breakup and cratonic underplating at rifted margins. Nature, 473(7345), 74-78.

Huisman, R. S., & Beaumont, C. (2014). Rifted continental margins: The case for depth-dependent extension. Earth and Planetary Science Letters, 407, 148-162.

Jackson, M. P. A., & Vendeville, B. C. (1994). Regional extension as a geologic trigger for diapirism. Geological society of America bulletin, 106(1), 57-73.

Jackson, M. P., & Hudec, M. R. (2005). Stratigraphic record of translation down ramps in a passive-margin salt detachment. Journal of Structural Geology, 27(5), 889-911.

Jackson, M.P., Hudec, M.R. (2017). Salt Tectonics: Principles and Practice. Cambridge University Press.

Jackson, C. A. L., Rodriguez, C. R., Rotevatn, A., & Bell, R. E. (2014). Geological and geophysical expression of a primary salt weld: An example from the Santos Basin, Brazil. *Interpretation*, 2(4), SM77-SM89.

Jackson, C. A. L., Jackson, M. P., Hudec, M. R. (2015a). Understanding the kinematics of salt-bearing passive margins: A critical test of competing hypotheses for the origin of the Albian Gap, Santos Basin, offshore Brazil. *Geological Society of America Bulletin*, 127(11-12), 1730-1751.

Jackson, C. A. L., Jackson, M. P., Hudec, M. R., Rodriguez, C. R. (2015b). Enigmatic structures within salt walls of the Santos Basin—Part 1: Geometry and kinematics from 3D seismic reflection and well data. *Journal of Structural Geology*, 75, 135-162.

Karner, G. D., Gambôa, L. A. P. (2007). Timing and origin of the South Atlantic pre-salt sag basins and their capping evaporites. *Geological Society, London, Special Publications*, 285(1), 15-35.

Krészsek, C., Adam, J. and Grujic, D (2007). Mechanics of fault and expulsion rollover systems developed on passive margins detached on salt: insights from analogue modelling and optical strain monitoring. *Geological Society, London, Special Publications*, 292(1), pp.103-121.

Kukla, P. A., Strozyk, F., & Mohriak, W. U. (2018). South Atlantic salt basins—witnesses of complex passive margin evolution. *Gondwana Research*, 53, 41-57.

Kumar, N., Danforth, A., Nuttall, P., Helwig, J., Bird, D. E., & Venkatraman, S. (2013). From oceanic crust to exhumed mantle: A 40 year (1970–2010) perspective on the nature of crust under the Santos Basin, SE Brazil. *Geological Society, London, Special Publications*, 369(1), 147-165.

Lebit, H., Arasanipalai S., Tilton, J. & Ollagnon, P. (2019) Santos Vision: Innovative Seismic Data Processing in a Super Giant Oil Basin. *GeoExPro*, May, 2019.

Lentini, M. R., Fraser, S. I., Sumner, H. S., & Davies, R. J. (2010). Geodynamics of the central South Atlantic conjugate margins: implications for hydrocarbon potential. *Petroleum Geoscience*, 16(3), 217-229.

Lewis, M. M., Jackson, C. A. L., & Gawthorpe, R. L. (2013). Salt-influenced normal fault growth and forced folding: the Stavanger Fault System, North Sea. *Journal of Structural Geology*, 54, 156-173.

Magee, C., Pichel, L. M., Madden-Nadeau, A., Jackson, C. A. L., & Mohriak, W. (2020). Salt-magma interactions influence intrusion distribution and salt tectonics in the Santos Basin, offshore Brazil.

Marton, L. G., Tari, G. C., & Lehmann, C. T. (2000). Evolution of the Angolan passive margin, West Africa, with emphasis on post-salt structural styles. *Geophysical Monograph-American Geophysical Union*, 115, 129-150.

Meisling, K. E., Cobbold, P. R., Mount, V. S. (2001). Segmentation of an obliquely rifted margin, Campos and Santos basins, southeastern Brazil. *AAPG bulletin*, 85(11), 1903-1924.

Modica, C. J., Brush, E. R., 2004. Postrift sequence stratigraphy, paleogeography, and fill history of the deep-water Santos Basin, offshore southeast Brazil. *AAPG bulletin*, 88(7), 923-945.

Mohriak, W.U., Macedo, J.M., Castellani, R.T., Rangel, H.D., Barros, A.Z.N., Latgé, M.A.L., Mizusaki, A.M.P., Szatmari, P., Demercian, L.S., Rizzo, J.G. Aires, J.R. (1995). Salt tectonics and structural styles in the deep-water province of the Cabo Frio region, Rio de Janeiro, Brazil, in: Jackson, M. P. A., Roberts, D. G., Snelson, S. (eds) *Salt tectonics: a global perspective*. AAPG Memoir 65, 273-304.

Mohriak, W., Nemčok, M., Enciso, G. (2008). South Atlantic divergent margin evolution: rift-border uplift and salt tectonics in the basins of SE Brazil. *Geological Society, London, Special Publications*, 294(1), 365-398.

Mohriak, W. U., Nóbrega, M., Odegard, M. E., Gomes, B. S., & Dickson, W. G. (2010). Geological and geophysical interpretation of the Rio Grande Rise, south-eastern Brazilian margin: extensional tectonics and rifting of continental and oceanic crusts.

Mohriak, W. U., Szatmari, P., Anjos, S. (2012). Salt: geology and tectonics of selected Brazilian basins in their global context. *Geological Society, London, Special Publications*, 363(1), 131-158.

Moulin, M., Aslanian, D., Rabineau, M., Patriat, M., & Matias, L. (2013). Kinematic keys of the Santos–Namibe basins. *Geological Society, London, Special Publications*, 369(1), 91-107.  
Norton, I. O., Carruthers, D. T., & Hudec, M. R. (2016). Rift to drift transition in the South Atlantic salt basins: A new flavor of oceanic crust. *Geology*, 44(1), 55-58.

Peel, F. J., Travis, C. J., & Hossack, J. R. (1995). Genetic structural provinces and salt tectonics of the Cenozoic offshore US Gulf of Mexico: A preliminary analysis.

Peel, F. J. (2014). The engines of gravity-driven movement on passive margins: Quantifying the relative contribution of spreading vs. gravity sliding mechanisms. *Tectonophysics*, 633, 126-142.

Péron-Pinvidic, G., & Manatschal, G. (2009). The final rifting evolution at deep magma-poor passive margins from Iberia-Newfoundland: a new point of view. *International Journal of Earth Sciences*, 98(7), 1581-1597.

Pichel, L. M., Peel, F., Jackson, C.A.-L., Huuse, M., 2018, Geometry and kinematics of salt-detached ramp syncline basins, *Journal of Structural Geology*, 115, 208-230. in press, doi: 10.1016/j.jsg.2018.07.016.



Pichel, L. M., Huuse, M., Redfern, J., & Finch, E. (2019a). The influence of base-salt relief, rift topography and regional events on salt tectonics offshore Morocco. *Marine and Petroleum Geology*, 103, 87-113.

Pichel, L. M., Finch, E., & Gawthorpe, R. L. (2019b). The Impact of Pre-Salt Rift Topography on Salt Tectonics: A Discrete-Element Modeling Approach. *Tectonics*, 38(4), 1466-1488.

Pichel, L. M., Jackson, C. A. L., Peel, F., & Dooley, T. P. (2019c). Base-salt relief controls salt-tectonic structural style, São Paulo Plateau, Santos Basin, Brazil. *Basin Research*.

Pichel, L. M., & Jackson, C. A-L., (2020a) Four-dimensional Variability of Composite Halokinetic Sequences. *Basin Research*.

Pichel, L. M., & Jackson, C. A. L. (2020b). The enigma of the Albian Gap: spatial variability and the competition between salt expulsion and extension. *Journal of the Geological Society*.

Pindell, J. L., & Kennan, L. (2007). Rift models and the salt-cored marginal wedge in the northern Gulf of Mexico: Implications for deep-water Paleogene Wilcox deposition and basinwide maturation. In *Perkins Research Conference Proceedings (Vol. 27, pp. 146-186)*.

Quirk, D. G., Schødt, N., Lassen, B., Ings, S. J., Hsu, D., Hirsch, K. K., Von Nicolai, C. (2012). Salt tectonics on passive margins: examples from Santos, Campos and Kwanza basins. *Geological Society, London, Special Publications*, 363(1), 207-244.

Quirk, D. G., Hertle, M., Jeppesen, J. W., Raven, M., Mohriak, W. U., Kann, D. J., ... & Mendes, M. P. (2013). Rifting, subsidence and continental break-up above a mantle plume in the central South Atlantic. *Geological Society, London, Special Publications*, 369(1), 185-214.

Roca, E., Muñoz, J. A., Ferrer, O., & Ellouz, N. (2011). The role of the Bay of Biscay Mesozoic extensional structure in the configuration of the Pyrenean orogen: Constraints from the MARCONI deep seismic reflection survey. *Tectonics*, 30(2).

Rodriguez, C. R., Jackson, C. L., Rotevatn, A., Bell, R. E., Francis, M. (2019). Dual tectonic-climatic controls on salt giant deposition in the Santos Basin, offshore Brazil. *Geosphere*, 14(1), 215-242.

Roma, M., Vidal-Royo, O., McClay, K.R., Ferrer, O., Muñoz, J.A. (2018a). Tectonic inversion of salt-detached ramp-syncline basins as illustrated by analog modeling and kinematic restoration. *Interpretation*, 6 (1), 127-144.

Rowan, M. G., Peel, F. J., & Vendeville, B. C. (2004). Gravity-driven fold-belts on passive margins.

Rowan, M. G., & Ratliff, R. A. (2012). Cross-section restoration of salt-related deformation: Best practices and potential pitfalls. *Journal of Structural Geology*, 41, 24-37.

Rowan, M. G. (2014). Passive-margin salt basins: Hyperextension, evaporite deposition, and salt tectonics. *Basin Research*, 26(1), 154-182.

Rowan, M. G. (2020). The South Atlantic and Gulf of Mexico salt basins: crustal thinning, subsidence and accommodation for salt and presalt strata. Geological Society, London, Special Publications, 476(1), 333-363.

Rowan, M. G., & Jarvie, A. (2020). Crustal extension and salt tectonics of the Danmarkshavn Ridge and adjacent basins, NE Greenland. *Marine and Petroleum Geology*, 104339.

Sclater, J. G., & Christie, P. A. (1980). Continental stretching: An explanation of the post-mid-Cretaceous subsidence of the central North Sea basin. *Journal of Geophysical Research: Solid Earth*, 85(B7), 3711-3739.

Scotchman, I. C., Marais-Gilchrist, G., Souza, F., Chaves, F. F., Atterton, L. A., Roberts, A., & Kuszniir, N. J. (2006). A failed sea-floor spreading centre, Santos Basin, Brasil. In *Rio Oil &*

Gas Expo and Conference. Rio de Janeiro, Brazil, Brazilian Petroleum, Gas and Biofuels Institute.

Scotchman, I. C., Gilchrist, G., Kusznir, N. J., Roberts, A. M., & Fletcher, R. (2010). The breakup of the South Atlantic Ocean: formation of failed spreading axes and blocks of thinned continental crust in the Santos Basin, Brazil and its consequences for petroleum system development. In Geological Society, London, Petroleum Geology Conference series (Vol. 7, No. 1, pp. 855-866). Geological Society of London.

Tari, G., & Jabour, H. (2013). Salt tectonics along the Atlantic margin of Morocco. Geological Society, London, Special Publications, 369(1), 337-353.

Tari, G., Novotny, B., Jabour, H., & Hafid, M. (2017). Salt tectonics along the Atlantic margin of NW Africa (Morocco and Mauritania). In Permo-Triassic Salt Provinces of Europe, North Africa and the Atlantic Margins (pp. 331-351). Elsevier.

Warren, J. K. (2016). Evaporites: A geological compendium. Springer.